UNEXPECTED SHIFT FROM PHYTOPLANKTON TO PERIPHYTON IN SMALL EUTROPHIC STREAMS OF THE NORTHERN GREAT PLAINS DUE TO WASTEWATER INFLUX

Nathanael T. Bergbusch[1,2], Nicole M. Hayes[1,2,3], Gavin L. Simpson[2], and Peter R. Leavitt[1,2,4,*]

[1] Limnology Laboratory, Department of Biology, University of Regina, Regina, Saskatchewan S4S 0A2 Canada

[2] Institute of Environmental Change and Society, University of Regina, Regina, Saskatchewan, S4S 0A2, Canada

[3] Present address: Biology Department, University of Wisconsin Stout, Menomonie, Wisconsin, 54751, USA

[4] Global Institute for Food Security, Queen's University Belfast, Belfast Antrim, BT9 5DL, United Kingdom

[*]Author for correspondence

Contacts:
NTB nbergbusch@gmail.com, ORCID 0000-0002-8062-6876
NMH hayesn@uwstout.edu; ORCID 0000-0002-5664-9939
GL Gavin.Simpson@uregina.ca, ORCID 0000-0002-9084-8413
PRL Peter.Leavitt@uregina.ca[1], P.Leavitt@QUB.ac.uk[4], ORCID 0000-0001-9805-9307

Keywords: periphyton, phytoplankton, biological nutrient removal, nitrate, NO_3^-, eutrophication, light, effluent, generalized additive models, HPLC, pigment, stream, river, prairie, northern Great Plains.

Running head: Effluent effects on periphyton and phytoplankton

Abstract

Pollution with nitrogen (N) and phosphorous (P) impairs streams by favouring suspended blooms of algae and cyanobacteria over diatom-rich periphyton. Recently, wastewater treatment plants (WWTP) have been upgraded to biological nutrient removal (BNR) to eliminate both P and NH_4^+, although little is known of the effects of BNR effluent on flowing waters. Here we compared the effects of BNR effluent with those of natural physico-chemical processes (hydrology, temperature, pH, conductivity, transparency) by analyzing changes in the abundance and composition of suspended (phytoplankton) and attached (periphyton) phototrophs in small, turbid, and P-rich streams of the northern Great Plains using high performance liquid chromatography. Generalized additive models (GAMs) explained 45.5-62.6% of deviance in temporal and spatial patterns in total phototroph abundance (as Chl a) and 77.5-86.5% of deviance in community composition (as biomarker carotenoids). Overall, phytoplankton were replaced by periphyton within WWTP-impacted reaches due to dilution of streams by transparent effluent. Further, phenology and composition of both periphytic and planktonic assemblages were altered, with increases in diatoms and chlorophytes in part due to abundant NO_3^- from effluent. Wastewater effects were limited to first-order reaches and normal patterns of seasonal succession were re-established in a downstream second-order river. Physico-chemical parameters explained similar deviance in GAMs of total abundance and community composition in both planktonic (65.2% and 82.5%, respectively) and epilithic habitats (40.5%, 72.5%). Overall, BNR appeared to shift turbid, phytoplankton-rich streams to boreal-like conditions with diatom-rich biofilms by improving water transparency and providing NO_3^- to diatoms and chlorophytes.

Scientific significance

After decades of focus on phosphorus control, wastewater treatment facilities are being upgraded worldwide to additionally remove nitrogen (mainly ammonium) from urban effluent, yet little is known of how a sudden change in wastewater processing may influence stream ecosystems. Here we measured changes in attached (periphyton) and suspended (phytoplankton) phototrophs in first- and second-order prairie streams over two years to evaluate the effects of urban effluent treated by biological nutrient removal (BNR) relative to the effects of natural landscape controls of lotic production (temperature, irradiance, dischange, water chemistry). Unexpectedly, inputs of BNR effluent reduced phytoplankton abundance and stimulated periphyton growth on rocks by both dilution of suspended communities and provision of moderate levels of nitrate (5 mg N L^{-1}) to periphyton. Resulting phototrophic communities resembled those found in unimpacted, restored, or boreal streams, suggesting that wastewater processing using BNR improved lotic ecosystem health by reducing cyanobacteria and favouring benthic diatoms and chlorophytes.

Introduction

Blooms of harmful algae and cyanobacteria negatively impact the health, function, and recreational value of aquatic ecosystems (Carpenter et al. 1998; Schindler 2006; Dodds et al. 2009), including reduced potability of drinking water supplies, depletion of dissolved oxygen, production of toxins, and decreased biodiversity (Paerl and Otten 2013). Harmful algal blooms (HABs) in freshwaters are forecast to increase globally during the 21st century due to climate change and nutrient pollution with nitrogen (N) and phosphorous (P) (Paerl and Paul 2012; Taranu et al. 2015; Vogt et al. 2018). Insights from algae and cyanobacteria in lotic ecosystems may be crucial in developing timely and effective remediation strategies, as nutrient pollution often starts in flowing waters associated with farms and urban centers (Grimm et al. 2008; Dodds and Smith 2017) where primary producers also integrate environmental changes within the catchment (Allan 2004; Walsh and Wepener 2009; Teittinen et al. 2015).

Both algae (Burliga and Kociolek 2016; Sherwood 2016) and cyanobacteria (Scott and Marcarelli 2012; Casamatta and Hašler 2016) are ubiquitous in streams (Giller and Malmqvist 1998), but mechanisms regulating their relative prevalence in the water column and on substrates are debated (Wu et al. 2011; Breuer et al. 2017). Blooms of suspended algae and cyanobacteria (phytoplankton herein) are common in higher-order rivers because of low canopy cover, high nutrient content, and long water residence time (Vannote et al. 1980; Reynolds and Descy 1996). In contrast, periphyton are typically the predominant primary producers in lower-order streams where canopy cover is common and water flows at a faster rate (Vannote et al. 1980; Biggs 1995; Biggs 1996). However, small eutrophic streams that lack vegetative canopies and have low discharge rates can also exhibit abundant metabolically-active phytoplankton (Waiser et al. 2011; Wu et al. 2011; Breuer et al. 2017). Depending on the local hydrology, these planktonic

communities may originate from sloughed periphyton, upstream lakes, or may exhibit a unique *in situ* composition; in all cases, the planktonic assemblage may act as an inoculum for downstream ecosystems (Roeder 1977; Bellinger and Sigee 2010). While the balance between periphyton and phytoplankton is well studied in larger lotic ecosystems (Van Nieuwenhuyse and Jones 1996; Chambers et al. 2012; Dodds and Smith 2017), less is known about suspended phototrophs in small eutrophic streams (Breuer et al. 2017).

Changes in the abundance, composition, and habitat of primary producers can be valuable indicators of human and climatic effects on lotic ecosystems (Allan 2004; Walsh and Wepener 2009; Teittinen et al. 2015). Excess nutrients can favour phototroph blooms (Biggs 2000; Chambers et al. 2012), as well as changes in the predominant taxa (Kelly and Whitton 1995; Walsh and Wepener 2009; Lobo et al. 2016) and habitat of production (Roeder 1977; Stevenson and White 1995), with benthic diatoms giving way to chlorophytes and potentially-toxic cyanobacteria in the water column (Baker and Humpage 1994; Affourtit et al. 2001; Mischke et al. 2011) and some benthic habitats (Peterson and Grimm 1992; Loza et al. 2013; McCall et al. 2017). However, despite clear distinctions between periphyton and phytoplankton in lotic ecosystems, controls of transition between habitats are rarely studied within a single stream (Roeder 1997; Breuer et al. 2017) despite the potential value of this metric as an early warning indicator of bloom development and eutrophication (Wurtsbaugh et al. 2019). For example, discrete inputs of anthropogenic nutrients and contaminants may cause substantial changes in streams (Peterson et al. 2001; Tank et al. 2018) that regulate the relative importance of attached or suspended phototrophs.

In principle, physico-chemical factors regulate both suspended and attached primary producers in flowing waters (Andrus et al. 2015; Breuer et al. 2017). Periphyton in small

streams are affected by changes to light (canopy cover, turbidity; Munn et al. 1989; Rosemond et al. 2000; Matthaei et al. 2010), temperature (Baker and Baker 1979; Munn et al. 2002; Wu et al. 2011), discharge (and scouring; Biggs 1995; Leland 2003), and nutrients (N and P; Tank and Dodds 2003; Breuer et al. 2017), as well as their interactions (Wu et al. 2011; Breuer et al. 2017). Less is known about the regulation of phytoplankton in small streams (Breuer et al. 2017), but in large rivers, nutrient effects may be paramount if light is sufficient (reduced canopy cover) and flow is slow (Reynolds and Descy 1996; Smith and Dodds 2017). Here low ratios of N:P may promote nitrogen-fixing cyanobacteria (Marcarelli et al. 2008; Smith and Dodds 2017), while variation in fluxes, stoichiometry, and chemical forms of N may cause taxa-specific variation in growth (Guildford and Hecky 2000; Klausmeier et al. 2004; Glibert et al. 2016). For example, diatoms and cryptophytes often nitrate (NO_3^-) over ammonium (NH_4^+) (Glibert et al. 2016, Swarbrick et al. 2019), whereas toxic cyanobacteria are favoured by intermediate concentrations of NH_4^+ (1-4 mg L^{-1}), and chlorophytes can predominate at extreme levels of N pollution (> 10 mg L^{-1}) (Bogard et al. 2020). Although well documented *in vitro* and in lakes, such taxon-specific responses have only recently been quantified in lotic systems (Varol and Sen 2018; Solomon et al. 2019; Kim et al. 2020), let alone in P-rich streams where the form and magnitude of N influx may dictate community composition.

Seasonal patterns of community development can both regulate and obscure physico-chemical controls of phototrophic abundance and community composition (Munn et al. 2002; Black et al. 2011; Andrus et al. 2013). Diatoms are adapted to cooler water (T_{min} 3-5 °C, T_{opt} 17-22°C; Paerl 2014), low irradiance, and moderately high turbulence, while chlorophytes (T_{opt} 27-32 °C) and cyanobacteria (T_{opt} 27-37 °C) generally prefer warm, stagnant, and high-irradiance conditions (Leland et al. 2001; Guven and Howard 2006; Visser et al. 2016; Swarbrick et al.

2019). Consequently, periphyton and phytoplankton often have enhanced diatom production in spring and fall in many lotic systems (Cattaneo et al. 1983; Andrus et al. 2013; Breuer et al. 2016), whereas chlorophytes and cyanobacteria may predominate in summer (Sommer et al. 2012; Breuer et al. 2016; Moorhouse et al. 2018). In theory, such seasonal phenology reflects concomitant changes in nutrients, hydrological discharge, temperature, and irradiance (Stevenson 1997; Savoy et al. 2019); however, in some instances, strong seasonality and climate effects can obscure, or be obscured by, effects of regional land use and point-source pollution (Andrus et al. 2013, 2015). Overall, the degree to which seasonal development of phototrophic communities interacts with anthropogenic changes in the biophysical environment of stream ecosystems is poorly understood, particularly for non-boreal systems (Dodds et al. 2004; Breuer et al. 2017).

This paper uses generalized additive models (GAMs) of physical and chemical parameters to identify the factors regulating temporal and spatial development of periphyton and phytoplankton assemblages in two small prairie streams. Wascana Creek receives treated urban effluent mid-reach before its confluence with the Qu'Appelle River. We measured variation in abundance and composition of phytoplankton and periphyton using taxonomically-diagnostic pigment biomarkers (chlorophylls [Chl], carotenoids) to quantify: 1) spatial and seasonal distribution of phototrophic biomass and community composition; 2) effects of wastewater treatment plant (WWTP) discharge on phytoplankton and periphyton, and; 3) how the relative abundance of suspended and attached communities varies with physico-chemical features of the streams and human influences. We hypothesized that: 1) primary producers would shift from spring diatoms to summer cyanobacteria in both suspended and attached communities (Sommer et al. 2012; Breuer et al. 2016; Moorhouse et al. 2018); 2) effects of urban effluent would overwhelm the seasonal phenology of periphyton (Davis et al. 1990; Rosemond et al. 2000;

Murdock et al. 2004) and phytoplankton (Giorgio et al. 1991; Biggs and White 1995; Solomon et al. 2019) at impacted sites; 3) NO_3^- from effluent would favour siliceous algae and chlorophytes over cyanobacteria downstream of WWTP discharge (Glibert et al. 2016; Swarbrick et al. 2019), and; 4) influx of urban effluent would alter ratios of periphyton:phytoplankton changing the *in situ* irradiance regime (Munn et al. 1989; Rosemond et al. 2000; Matthaei et al. 2010).

Methods

Study area

Study sites consisted of first-order Wascana Creek (WC) and second-order Qu'Appelle River (QR), small streams within the northern Great Plains of southern Saskatchewan, Canada (Fig. 1, Table 1). The QR drainage basin covers ~52,000 km^2 of intensive agriculture (mainly wheat, canola) and more limited natural grassland, wetland, and urban environments (Hall et al. 1999b; Patoine and Leavitt 2006). Regional climate is a cool-summer humid continental regime (Köppen D*fb*), with high seasonal variation, short summers (July mean of 19 °C), cold winters (January mean of -16 °C), and low-annual temperatures (~ 1.5 °C) (Leavitt et al. 2006; Swarbrick et al. 2019). Wascana Creek is a naturally-intermittent prairie stream draining ~ 1400 km^2 in a northwest direction through Wascana Lake and the City of Regina, before receiving treated effluent from a biological nutrient removal (BNR) facility. Overall, urban effluent was high in nitrate, but not NH_4^+ or soluble reactive P (SRP), whereas the natural lotic discharge exhibited relatively high P, turbidity, and organic N (Leavitt et al. 2006; Waiser et al. 2011; Bogard et al. 2012). Wascana Creek continues northwest ~65 km before its confluence with the Qu'Appelle River, a misfit stream flowing east to Pasqua Lake (Leavitt et al. 2006). The QR originates in wetlands near Eyebrow Lake west of Regina and flows eastward though eutrophic Buffalo Pound Lake before its confluence with WC (Fig. 1). Flow in the QR is also

supplemented year-round by water discharged from the mesotrophic Lake Diefenbaker reservoir and, in late summer of most years, by flow from eutrophic, sub-saline Last Mountain Lake immediately northeast of the WC-QR confluence. Catchment hydrology is detailed in Haig et al. (2020).

Both WC and QR are naturally small, turbid, alkaline, and P-rich streams, often exhibiting N limitation and abundant suspended cyanobacteria by late summer (Waiser et al. 2011; Supporting Information Fig. S1). Discharge in both systems exhibits high seasonality, with spring snow melt accounting for 80% of surface runoff (Pomeroy et al. 2007; Pham et al. 2009; Haig et al. 2020). Flow is limited during winter and much of summer, particularly in WC where the WWTP makes up most of the discharge during June to September and November to March (Waiser et al. 2011). Nutrient retention is highly variable by season and compound, with an uptake length ranging: ~120 km (July) to ~50 km (May) for SRP; ~10 km (July) to ~70 km (May) for NH_4^+, and; ~300 km (July) to ~0 km (May) for NO_3^- (Waiser et al. 2011). Rapid nitrification of NH_4^+ to NO_3^- (Waiser et al. 2011), as well as denitrification and nitrous oxide emissions (Dylla 2019), also occur below the wastewater outfall. Presently, mean (± SE) effluent nutrient levels include 5.8 ± 0.07 mg N L^{-1} as NO_3^-, 1.82 ± 0.07 mg N L^{-1} as NH_4^+, and 0.58 ± 0.02 mg P L^{-1} as TDP (Table 1).

Field methods

Nine stations were sampled along the continuum formed from WC headwaters to QR near Pasqua Lake (Fig. 1), including two sites upstream of the WWTP outfall (before and after Wascana Lake), three stations between the WWTP outfall and the WC-QR confluence, and four locations along the mainstem of the QR (upstream of confluence, upstream of Last Mountain Lake inflow, two further downstream). All sites were sampled bi-weekly 01 May to 15

September 2018 and 2019 between 9:00 and 14:00 hrs. At each station, temperature (°C), cloud cover (%), and wind velocity (km s^{-1}) were recorded, while a YSI Model 85 meter was used to register water temperature (°C), dissolved oxygen (mg O_2 L^{-1}), specific conductivity (µS cm^{-1}), salinity (g total dissolved solids [TDS] L^{-1}), and pH at surface, mid-column, and near-bottom depths. Surface values were used for subsequent analyses, as there was limited variation with water-column position. Water transparency was recorded with a 20-cm diameter Secchi disk, as well as a LaMotte model 2020we turbidity meter.

On each date, a 10-L sample of water was collected from each site from near the stream centre by integrating discrete samples from surface to mid-column depths using a sterile container. Water was screened though a 243-µm pore mesh to remove invertebrates and particulate matter, but not phytoplankton (Vogt et al. 2018). Periphyton samples at each location were collected from the stream side at approximately 10-cm water depth by using a sterile brush to remove three similar-sized biofilms of known area (~5 cm diameter) from rocks randomly chosen from a standard cobble deposit. Periphyton samples were diluted with deionized water, and stored in sterile Whirl-Pak® bags for transportation. Although subject to potentially greater variability (Morin and Cattaneo 1992), we used natural substrates to both better capture the normal phenological patterns of these prairie streams, and to avoid the underestimation of total periphyton, chlorophytes, and cyanobacteria abundances commonly associated with use of artificial surfaces (Cattaneo and Amireault 1992). We measured instantaneous water velocity, water-column depth, and channel cross-sectional area at wade-able sites (< 1.2 m depth) using a calibrated Swoffer Instruments Inc. model 2100 current velocity meter, following the two-point (> 0.75 m) and $6/10^{th}$ (< 0.75 m) depth methods of Buchanan and Somers (1976). All samples were processed in the laboratory before 17:00 hrs on day of collection. In addition, we collected

weekly discrete (instantaneous) and 24-h integrated samples of treated wastewater effluent from EPCOR Utilities for the period of May 2018 to August 2019.

Laboratory methods

Whole-water and periphyton samples were filtered through GF/C glass fibre filters (1.2 µm nominal pore size) and stored frozen at -20 °C until later analysis of pigments and stable isotopes. Filtrate was then passed through 0.45-µm pore membrane filters and frozen at -20 °C until analysis for soluble nutrient concentrations. GF/C filters were used for pigment and POM analyses.

Concentrations of ammonia (NH_3) /ammonium (hereafter as NH_4^+), nitrite (NO_2^-) /nitrate (hereafter as NO_3^-), total dissolved nitrogen (TDN), SRP, and total dissolved phosphorous (TDP) were analyzed using a Lachat QuikChem 8500 FIA automated ion analyzer and standard procedures (APHA-AWWA/WEF 1998) at the Institute of Environmental Change and Society (IECS), University of Regina. In addition, the City of Regina supplied monthly estimates of NH_4^+, NO_2^-, NO_3^-, TDN, and TDP collected near our sites, as well as at additional locations. Finally, nutrient concentrations in treated effluent from the Regina WWTP were supplied by EPCOR Utilities (Edmonton, Canada). All N and P species were expressed as mg nutrient L^{-1}.

Stable isotopes of carbon (C) and N from filtered water, effluent, particulate organic matter, and periphyton were measured for all sampling sites using the protocols of Leavitt et al. (2006). Briefly, GF/C-filtered water and effluent samples were freeze-dried (1 week, 0.01 Pa) to obtain residue for analysis, whereas POM and periphyton filters were dried in an oven at 66 °C for 24 h. We packed 10-15 mg of solids from treated effluent or wastewater-impacted river sites, whereas 20-25 mg was used for isotope analysis of undisturbed sites. Different masses were needed to optimize N content for combustion and elemental analysis. We used six 6-mm

diameter hole-punches of GF/C filters for stable isotope analysis of POM and periphyton. All solids were folded into individual tin capsules and combusted in a NC2500 Elemental Analyzer (ThermoQuest, CE Instruments) coupled to a Thermoquest (Finnigan-MAT) Delta PlusXL isotope ratio mass spectrometer (IRMS). Stable isotope values are presented using standard expressions ($\delta^{13}C$, $\delta^{15}N$) calibrated relative to atmospheric and laboratory standards, whereas elemental content was expressed as % dry mass (% C, % N).

Total abundance and community composition of phytoplankton and periphyton were estimated using standard trichromatic spectrophotometric analysis of Chl a (Jeffrey and Humphrey 1975) and high-performance liquid chromatography (HPLC) quantification of biomarker pigments (Leavitt and Hodgson 2001; Steinman et al. 2017), respectively. Briefly, filters were completely extracted with either HPLC-grade acetone (trichromatic Chl a) or acetone, methanol, and water in a ratio of 80:15:5 by volume (all pigments and derivatives) for 24 h at -20 °C, then filtered (0.2-µm pore membrane) before further processing. Samples for HPLC analysis were dried in the dark under nitrogen (N_2) gas and stored at -80 °C until pigments were redissolved into a standard injection solvent mixture containing a Sudan II chromatographic standard (Leavitt and Hodgson 2001). HPLC samples were processed using an Agilent 1100 HPLC equipped with a model 1100 photodiode array and fluorescence detector. The HPLC system was calibrated with authentic standards from DHI Denmark Inc. and other local reference sources following Leavitt and Hodgson (2001).

Pigments were tentatively identified on the basis of absorbance spectra and chromatographic position. Biomarker pigments included both carotenoids and chlorophylls such as Chl a and β-carotene (total phytoplankton), fucoxanthin (siliceous algae and some dinoflagellates), diadinoxanthin (diatoms, dinoflagellates, some chrysophytes), diatoxanthin

(mainly diatoms), peridinin (dinoflagellates), alloxanthin (cryptophytes), Chl b (chlorophytes), lutein-zeaxanthin (chlorophytes and cyanobacteria), myxoxanthophyll (colonial cyanobacteria), canthaxanthin (Nostocales cyanobacteria, potentially N_2-fixing), aphanizophyll (N_2-fixing cyanobacteria), and echinenone (total cyanobacteria). Lutein from green algae and zeaxanthin from cyanobacteria were not separated on our HPLC systems and are presented together as 'bloom-forming taxa'. Phytoplankton pigments from HPLC analysis were expressed as nmoles pigment L^{-1}, whereas periphytic biomarkers were estimated as nmoles pigment cm^{-2}. In addition, trichromatic Chl a was expressed as µg Chl a L^{-1} or µg Chl a cm^{-2}, consistent with protocols in the Qu'Appelle long-term ecological research program (QU-LTER; Vogt et al. 2011). We also calculated the ratio of labile Chl a to its stable degradation product, pheophytin a, to evaluate whether pigments represented live material or detritus. As ratios were routinely greater than 15:1 in both phytoplankton (17.01 ± 0.83) and epilithon (17.16 $\pm$ 1.04), we assumed that pigments mainly represented metabolically-active phototrophs (Leavitt 1993).

Ratios of periphyton to phytoplankton abundance were calculated by dividing volumetric estimates of planktonic pigments by aerial estimates of periphytic biomarkers. This mass ratio was used as an approximation of spatial and temporal changes in the relative abundance of primary producers in planktonic and attached habitats, even though it is recognized that comprehensive quantification of phototrophs would require integration of water-column and substrate-associated pigments from across the full suite of stream depths at each site. Such comprehensive sampling was beyond the capacity of this project, given the number of sites and difficulty accessing deeper benthic habitats (> 1 m depth). Nonetheless, comparison of absolute and relative changes in phototrophic communities using pigments is expected to provide insights on mechanisms regulating the abundance and relative composition of the two assemblages

(Vinebrooke and Leavitt 1999; Thomas et al. 2013), particularly given the high degree of spatial and temporal variation among sites.

Hydrometric data

Stream discharge was either directly measured, recorded by gauging stations, or calculated using the drainage area ratio method depending on seasonal flow and site characteristics. At wade-able sites, we calculated instantaneous discharge rate (Q) by summing the product of discrete velocities and their respective cross-sectional areas measured at 10-15 points along an orthogonal transect across the creek, following the two-point and 6/10th methods (Buchanan and Somers 1976). In all years, we also collected Q for sites with provincial and federal hydrometric real-time gauging stations, or applied the drainage area ratio method to estimate prorated discharge ($Q_{incremental}$) based on the nearest gauging station, incremental effective drainage area (EDA), and any additional tributaries and point-sources (Gianfagna et al. 2015; Swarbrick 2017). We note that the drainage area ratio method omits travel time, evaporation, and groundwater inputs or losses. $Q_{incremental}$ was calculated by multiplying the nearest gauging station (Q_{gauged}) by the ratio of the EDA between the sampling site and the gauged site ($A_{incremental}$) and the EDA of the gauged site (A_{gauged}), as follows:

$$Q_{incremental} = Q_{gauged} * (A_{incremental}/A_{gauged}).$$

The EDA of each sampling site, defined as the maximum area that could contribute flood runoff (Mowchenko and Meid 1983), was determined following Swarbrick (2017) by either using the federal Agricultural and Agri-Food Canada (AAFC) Watersheds Project dataset (2008), or calculated from the AAFC EDA total boundary layer, topographic and hydrologic data using ESRI ArcGIS 10.1 (Natural Resources Canada 2016). Finally, to validate all methods, we compared our *in situ* measured discharge rates with those estimated for the same site using either

316 governmental instrumentation or calculated via the drainage area ratio method (Supporting
317 Information Fig. S2). Although highly correlated (slope = 0.84, R^2_{adj} = 0.856, $P < 0.0001$), our
318 direct measurements tended to underestimate calculated discharge by about 0.75 $m^3 s^{-1}$ at flows
319 between 1 and 8 $m^3 s^{-1}$.

320 *Numerical analyses*

321 We used GAMs to estimate linear and non-linear spatio-temporal trends in phytoplankton
322 and periphyton assemblages and responses to physico-chemical variables (Pederson et al. 2019).
323 We used trichromatic Chl a as a proxy for total abundance of phototrophs and included the
324 following biomarker pigments in our community models: fucoxanthin (siliceous algae),
325 alloxanthin (cryptophytes), chlorophyll b (chlorophytes), and echinenone (total cyanobacteria).
326 Other pigments were not included in the main models either because compounds were rare (e.g.,
327 peridinin) or exhibited significant taxonomic overlap with selected biomarkers (e.g.,
328 cyanobacterial carotenoids). Additionally, Chl a derived from HPLC was modelled for
329 comparison with trichromatic Chl a. The QR site immediately upstream of the WC-QR
330 continuum was excluded from GAMs but was analyzed separately to better identify the
331 mechanisms contributing to downstream patterns in the QR.

332 Spatio-temporal models included a fixed effect of year, marginal smooth terms for day of
333 year (DOY) and distance along the stream flow path, plus a smooth interaction for DOY and
334 distance that allowed for seasonal difference along our lotic continuum. Distance and DOY
335 terms also included a tensor product smooth of year to allow for year-specific effects.
336 Additionally, pigment spatio-temporal models included DOY and distance factor-smoothers for
337 pigment-specific responses. We chose variables in physico-chemical models based on biological
338 relevance, while testing for both instantaneous and lag effects. Due to weak explanatory power,

we chose to omit time lags but retained effects of distance, DOY, discharge, pH, dissolved nutrients (NO_3^-, NH_4^+, SRP), the mass ratio of TDN to SRP, Secchi transparency, specific conductance, and temperature. Turbidity was removed from models because of substantial negative correlation with Secchi depth that reduced model performance. To achieve better dispersion of the data, NO_3^-, NH_4^+, TDN:SRP, turbidity, and specific conductance were $\log_{10}$-transformed, whereas SRP and discharge were square-root transformed. This analysis considered multi-collinearity of covariates prior to model creation by estimating the Pearson correlation coefficient for all pairs of predictors and concurvity of model smooths; no Pearson correlation was > 0.35, but smoother concurvity was high (0.7-0.9) suggesting non-linear correlation of parameters. To address non-linear correlations and to achieve best fit and parsimony, we penalized the range and null space of the smoothing matrices for physico-chemical variables during fitting with the option *select = true* (Marra and Wood 2011).

All models were run within the R statistical environment (v. 3.6.2; R Core Team 2018) with *mgcv* (v. 1.8-29; Pedersen et al. 2019) package with automatic smoothness estimation (Wood 2011; Wood et al. 2017). Prior to model creation, a redundancy analysis (RDA) was performed using the *vegan* package (v. 2.5-6; Oksanen et al. 2019) with physico-chemical constraints to determine initial linear relationships between pigments and physico-chemical covariates. Axes explained little variance (< 20%) and after variable selection (forward, backwards elimination, etc.), most biologically-relevant covariates were removed from the RDA, a pattern which suggests that underlying relationships were non-linear in nature. We used a gamma distribution (positive, continuous responses) with a log-link function for Chl a models because concentrations were > 0 µg L^{-1}. However, because concentration of other biomarker pigments were occasionally below detection limits (< 0.002 nmole pigment L^{-1}, cm^{-2}), a Tweedie

distribution (zero-inclusive, positive, continuous responses) was used for those models. We did not treat these observations as censored because < 1% of values were 0 and likely truly absent (0.0 nmole pigment L^{-1}) and because preliminary analysis with Bayesian regression models using *Stan* (BRMS, v. 2.10.0; Bürkner 2018) greatly overestimated observed pigment concentrations (i.e., exhibited a poor fit relative to *mgcv* models). In addition, models dealt with missing values internally by omitting data where physico-chemical variables were missing.

GAMs for pigment included global (all pigments) and pigment-specific smooth terms. Global terms were tensor-product smoothers, whereas pigment-specific terms were factor smoothers (Pedersen et al. 2019). We compared model residuals against physico-chemical parameters to determine which variables required taxa-specific response; all pigment models exhibited a substantial decrease in the magnitude of residuals and better homogeneity when taxa-specific responses were included. We assessed basis size, dispersion of residuals, homogeneity of variance, and the relationship between the observed and predicted response for all models to evaluate whether model assumptions were violated. Residual maximum marginal likelihood (REML) was used for smoothness selection (Wood 2011). Spatio-temporal model predictions and physico-chemical model marginal smooths were visualized in R using *ggplot2* (v. 3.2.1; Wickham 2016).

Results

Stream conditions

Physico-chemical conditions varied substantially from the headwaters of Wascana Creek (WC) to the downstream reaches of the Qu'Appelle River (QR) in both 2018 and 2019 (Table 1, Fig. 2). Headwaters immediately above the WWTP outfall were usually slow-flowing (< 1 $m^3 s^-$

384 ^{1}), moderately turbid (25-50 NTU), opaque (Secchi < 25 cm), alkaline (pH > 8.5), and relatively
385 ion-poor (specific conductance ~1000 µS cm^{-1}), with low concentrations of TDN (< 1 mg N L^{-1})
386 and relatively elevated levels of P (0.1 – 0.5 mg P L^{-1}) resulting in low TDN:SRP mass ratios
387 (13.8 ± 2.7) compared to other reaches (Table 1). Overall, the presence of Wascana Lake
388 between the two headwater sites appeared to have little effect on overall conditions, other than
389 leading to a sharp decline in dissolved P fractions, water transparency, and conductivity, and a
390 modest increase in pH and TDN:SRP ratios.

391 Influx of urban effluent altered the physico-chemical profile of WC and, to a lesser
392 extent, the QR, with particularly marked effects in 2018 (Fig. 2). Effluent was circumneutral
393 (7.42 ± 0.01 pH) and contained high concentrations of NO_3^- (5.80 ± 0.07 mg N L^{-1}) relative to
394 NH_4^+ (1.82 ± 0.07 mg N L^{-1}) and TDP (0.58 ± 0.02 mg P L^{-1}), with relatively low C:N ratios
395 (4.98 ± 0.11) and strongly enriched ^{15}N isotope values (16.82 ± 0.28 ‰) (Table 2.1, Supporting
396 Information Fig. S3). When combined with WC streamflow, effluent outfall led to substantial
397 increases in dissolved N concentrations (TDN, NO_3^-, NH_4^+), discharge, and water transparency
398 (increased Secchi depth, reduced turbidity). Further, $\delta^{15}N$ values for filtered whole water from
399 WC increased from regional baselines of 3 - 6 ‰ to 18 - 23 ‰ in all seasons (Fig. 2). In
400 contrast, pH declined sharply to ~8, whereas influx of effluent had more limited effects on
401 stream temperature and dissolved P concentrations (Fig. 2). Due to changes in the nutrient
402 regime following WWTP outfall, TDN:SRP mass ratios increased to > 23:1 (Fig. 2), suggesting
403 either phosphorous limitation of phototrophs or, more likely, saturation of nutrient demands
404 (Supporting Information Fig. S1). For many parameters (except Q, $\delta^{15}N_{water}$, SRP), effects of
405 effluent influx diminished with distance downstream, with a return to near-headwater conditions
406 just prior to the confluence of WC with the QR (Fig. 2).

Lotic environments changed again when WC emptied into the QR (Fig. 2). Discharge (> 2.5 $m^3 s^{-1}$) and often turbidity (10-60 NTU) reached maximal values, while water transparency often diminished to a minimum (Secchi < 20 cm, elevated turbidity), and other parameters returned to background levels characteristic of headwater and regional conditions (pH, salinity, specific conductivity). In general, elevated nutrient concentrations and $\delta^{15}N$ values in WC waters declined after the QR confluence, with particularly marked dilution of dissolved N compounds. Together, these patterns suggest that most pronounced physico-chemical effects of urban effluent influx were restricted to WC immediately below the WWTP outfall.

Spatio-temporal distribution of stream phototrophs

Analysis of trichromatic Chl a using GAMs revealed the presence of strong spatial-temporal patterns of primary producer abundance (Fig. 3). GAMs using year, distance, DOY, and their interaction explained 62.6%, 45.5%, and 53.9% of deviance in phytoplankton, periphyton, and periphyton:phytoplankton mass ratios, respectively. All predictive terms were significant ($p < 0.05$), except in the ratio model where only distance and DOY were retained (Fig. 3). Together, GAMs suggest that phototrophic communities exhibited marked variation among headwater, effluent-impacted, and post-confluence reaches, but that these patterns also exhibited seasonal variability (see below).

Phytoplankton and epilithon exhibited markedly different spatial patterns of abundance (as Chl a) along the continuum formed by WC and the QR (Fig. 3). In both years, total phytoplankton in headwaters increased to a peak downstream of Wascana Lake, declined following receipt of urban effluent, and increased after confluence with the already-turbid QR (Fig. 3a). In general, phytoplankton patterns were more pronounced during 2018 than in 2019, with GAMs revealing significant decreases in Chl a associated with wastewater influx in both

July and August 2018, but not during May and June 2018. In contrast, periphyton abundance increased sharply after WWTP inputs, before decreasing downstream of the confluence (Fig. 3b). In this case, GAMs showed that periphyton only increased significantly after the WWTP in 2019. GAMs also revealed a significant and substantial increase in periphyton:phytoplankton ratios downstream of the WWTP in both years and all seasons (Fig. 3c). Very similar spatial patterns of change were recorded for both phytoplankton and epilithon assemblages when analyzed with Chl a from HPLC (Supporting Information Fig. S4).

Phytoplankton and periphyton assemblages exhibited substantial variation in community composition from headwaters, through effluent-impacted reaches, to downstream habits within the QR (Fig. 4). Community GAMs explained high proportions of deviance for phytoplankton (86.5%), periphyton assemblages (81.1%), and their ratios (77.5%), with significant effects of distance, DOY, and their interaction in each case. Both suspended and benthic communities exhibited a high abundance of siliceous algae (as fucoxanthin) at most stations, with more site-specific additional contributions from cryptophytes (alloxanthin), chlorophyes (Chl b), and total cyanobacteria (echinenone). Furthermore, HPLC analysis revealed that planktonic cyanobacteria routinely consisted of colonial forms (as myxoxanthophyll) in all reaches, whereas periphytic cyanobacteria also included N_2-fixing Nostocales (canthaxanthin) and colonial forms (myxoxanthophyll) in WC headwaters and downstream QR reaches (Supporting Information Fig. S5). Comparison of mass ratios revealed that individual periphyton groups increased relative to phytoplankton downstream of the WWTP during late summer during 2018 (July – August) in spring, but during early summer (May - June) in 2019 (Fig. 4).

Spatial variation in the abundance of individual algal and cyanobacterial groups differed among years (Fig. 4), similar to patterns recorded with trichromatic Chl a (Fig. 3). In general, all

phytoplankton groups increased between the two headwater stations, before declining markedly downstream of the WWTP, particularly in the case of cryptophytes and total cyanobacteria. In contrast, abundance of siliceous algae and chlorophytes increased below the effluent outfall in spring and early summer of 2018. While these latter patterns were significant in that year, the abundance of all planktonic groups typically increased downstream of the confluence with the QR in both years (Fig. 4a). Unlike phytoplankton, abundance of all epilithon groups increased significantly in urban-impacted waters in 2019, with more limited increases observed in 2018 for cryptophytes and cyanobacteria in late summer. Abundance of periphyton usually declined within 25 km of wastewater outfall and remained low following the confluence of WC and QR, with the exception of attached cryptophytes (Fig. 4b) and colonial diazotrophic cyanobacteria (Supporting Information Fig. S5) which also increased in the furthest downstream reaches during 2019. In addition, the increase in the ratio of periphyton:phytoplankton was generally attributable to benthic chlorophytes and cyanobacteria in 2018 and benthic siliceous algae, cryptophytes, and chlorophytes in 2019 (Fig. 4c). Overall, these patterns suggest that influx of urban effluent favoured chlorophytes and siliceous algae in both habitats, while cyanobacteria were more common in WC headwaters and the larger QR ecosystem, sites with less urban impact.

Seasonality

Phytoplankton and periphyton exhibited opposite patterns of seasonal abundance in each year (Fig. 3). In 2018, phytoplankton exhibited a spring maximum and a summer minimum, whereas periphyton exhibited a summer maximum and a spring minimum. However, these patterns were reversed during 2019; periphyton had a spring maximum and a summer minimum, whereas phytoplankton had a spring minimum and a summer maximum. In addition, the

476 periphyton:phytoplankton ratio was highest during summer in 2018, but was maximal in spring
477 of 2019 (Fig. 3). In general, spring maxima of both phytoplankton and periphyton occurred in
478 the effluent-influenced portions of WC, as did summer peaks of epilithon, whereas summer
479 maxima occurred downstream of the WC–QR confluence (Fig. 3).

480 Predominance of individual algal and cyanobacterial groups also varied substantially
481 among seasons (Fig. 4, Supporting Information Fig. S5). During 2018, individual phototrophs
482 were generally more abundant in mid-to-late summer in turbid waters characteristic of headwater
483 and post-confluence reaches, whereas abundance of each group was usually higher in spring and
484 early summer in effluent-influenced sections of WC. Seasonal patterns were less distinct in
485 2019, other than cyanobacteria were most common in late summer at most sites, and all
486 phytoplankton groups exhibited higher seasonal abundance in August downstream of the
487 confluence (Fig. 4a). Fewer patterns were recorded in epilithic assemblages, beyond increased
488 abundance of cyanobacteria in late summer at many locations, and both May and August peaks
489 of algal and cyanobacterial groups in the effluent-influenced section of WC (Fig. 4b). Benthic
490 cyanobacteria and chlorophytes were responsible for an increase in the ratio of
491 periphyton:phytoplankton in 2018, whereas in 2019 this was attributable to siliceous algae,
492 chlorophytes, and cryptophytes. In general, colonial cyanobacteria (as myxoxanthophyll),
493 including potentially N_2-fixing forms (as canthaxanthin, aphanizophyll) were more common in
494 late summer in all reaches and habitats of the fluvial system (Supporting Information Fig. S5).
495 Taken together, these patterns suggest that for both phytoplankton and periphyton, WWTP inputs
496 favoured spring peaks of siliceous algae, chlorophytes, and some cryptophytes, while hindering
497 late-summer growth peaks, particularly of cyanobacteria.

Response of stream phototrophs to physico-chemical conditions

Analysis of trichromatic Chl a using GAMs suggested that phytoplankton and periphyton assemblages were regulated differentially by changes in physico-chemical conditions of flowing waters (Fig. 5). Overall, GAMs explained 66.3% of deviance for total phytoplankton and 53.9% for total epilithon, with significant effects ($p < 0.05$) of distance downstream (both communities) and DOY (phytoplankton only). For phytoplankton, total abundance increased with discharge, specific conductance, and secondarily NH_4^+ concentration, but declined with elevated Secchi depth, NO_3^- levels, and SRP content (Fig. 5a). In contrast, modelled periphyton abundance increased significantly ($p < 0.05$) with NH_4^+ concentrations, and declined with elevated discharge, extreme Secchi depth, and, more marginally, pH (Fig 5b). Effects of water temperature and TDN:SRP ratios were not significant ($p > 0.1$) in either habitat (smooth linear and flat, EDF ~ 0). In addition, similar models that did not include landscape position (distance from WWTP) and DOY explained slightly less deviance for both phytoplankton (64.1%) and epilithon (28.3%) models, although relationships between trichromatic Chl a and stream parameters were similar (analysis not shown).

Analysis of HPLC-derived pigments using GAMs explained 84.0% of deviance for phytoplankton assemblages, and 72.6% for periphyton communities when both years were analysed together (Fig. 6) or separately (analysis not shown). Within the phytoplankton model (Fig. 6a), significant global effects ($P < 0.05$; all biomarkers together) were recorded for all chemical (except pH) and physical variables, as well as spatial (distance) and temporal (DOY) parameters, while significant taxon-specific effects were included for all variables, except pH (marginal effect) (Fig. 6a). Similarly, most physico-chemical parameters exhibited significant global effects on epilithic assemblages (except temperature, SRP, and, marginally, TDN:SRP),

521 while taxon-specific effects were recorded for all parameters except discharge and, marginally,
522 NO_3^- (Fig. 6b).

523 Physico-chemical factors had differential effects on phototrophs. High discharge regimes
524 favoured elevated phytoplankton abundance but reduced densities of periphyton with limited
525 group-specific effects in either habitat (Fig. 6). However, unlike GAMs with trichromatic Chl a,
526 the irradiance regime did not have a consistent global effect on the response of phytoplankton
527 and periphyton assemblages to changes in illumination (Figs. 5, 6). In general, phytoplankton
528 generally declined as Secchi depth increased, whereas periphyton were largely unresponsive.
529 Responses of assemblages were generally most marked at Secchi depths > 90 cm, when
530 phytoplankton increased and periphyton declined. Group-specific effects of siliceous algae and
531 chlorophytes were usually greater than those of other phototrophs for both metrics of water
532 clarity.

533 Unlike Chl a (Fig. 5), periphyton exhibited a significant response to changes in pH when
534 analysed with all biomarker pigments (Fig. 6). Specifically, global effects of pH had minimal
535 effect on phytoplankton, whereas periphyton declined with pH (Figs. 5, 6). Overall group-
536 specific effects of chlorophytes were paramount in attached communities, whereas effects of
537 siliceous algae within the phytoplankton increased at the expense of green algae as pH increased.
538 In general, lower pH values were characteristic of reaches receiving urban effluent (Fig. 2).

539 The global response of phytoplankton biomarkers exhibited a unimodal relationship with
540 specific conductance, whereas that of periphyton increased with conductivity (Fig. 6). Again,
541 both responses were somewhat different than those recorded for Chl a alone, particularly for
542 epilithon (Fig. 5), and group-specific effects of chlorophytes and siliceous algae were
543 consistently greater than those of cryptophytes and total cyanobacteria.

Temperature had few pronounced global effects on phototrophs, other than somewhat diminished impacts on phytoplankton under extreme thermal regimes (< 10, > 25 ^{o}C). Overall, chlorophytes and siliceous algae exhibited stronger group-specific effects than other groups, particularly in the phytoplankton.

In general, phytoplankton and periphyton assemblages exhibited contrasting relationships to concentrations of dissolved nutrients (Fig. 6). For example, dissolved N species generally had their greatest global effects at moderate concentrations, but diminished effects on periphyton under intermediary conditions. Overall, phototrophic responses reflected elevated effects of chlorophytes or siliceous algae in both habitats. Effects of SRP were indistinct in both habitats, with more pronounced changes in siliceous algal effects than observed for other parameters. Global effects of TDN:SRP ratios on phytoplankton increased strongly with mass ratio, whereas those on epilithon declined, largely reflecting the predominant group-specific effects of chlorophytes and siliceous algae.

Discussion

Mechanisms affecting eutrophication of stream and river ecosystems can be difficult to discern due to complex interactions between natural controls (temperature, discharge, light, nutrients) and anthropogenic activities (Reynolds and Descy 1996; Dodds and Smith 2017; Bernhardt et al. 2018), particularly in less-well studied small eutrophic streams (Waiser et al. 2011; Wu et al 2011; Breuer et al. 2017). Here we contrasted the reach-specific effects of effluent from a WWTP (NO_3^--rich; low NH_4^+, reduced SRP, low turbidity) with natural physico-chemical processes as mechanisms regulating abundance and composition of algae and cyanobacteria in small productive prairie streams. Diverse phytoplankton were common in headwater and second-order reaches, with generally elevated densities in late summer (July-

August) (Figs. 3, 4; Supporting Information Fig. S5), reflecting favourable environmental conditions for primary production (Fig. 2) (Stevenson and White 1995) and, likely, inoculation from upstream waters (Qu et al. 2019).

Overall, abundances of phytoplankton and periphyton were inversely related (Fig. 3), with suspended communities often exhibiting pronounced N limitation in summer in headwaters and downstream regions (Supporting Information Fig. S1). Unexpectedly, influx of N-rich urban wastewater both reduced phytoplankton abundance and increased that of epilithon (Fig. 3), although the timing of greatest effect varied between 2018 (May-June) and 2019 (July-August). Anticipated seasonal phenology of community composition from diatoms to cyanobacteria (Sommer et al. 2012; Breuer et al. 2016; Moorhouse et al. 2018) was altered within effluent-impacted reaches to favour increased siliceous algae (mainly diatoms) and chlorophytes in both suspended (mainly in 2018) and attached habitats (2019), instead of cyanobacteria (Davis et al. 1990). Analysis of total phototrophic abundance (Fig. 5) or community composition (Fig. 6) with GAMs suggested that phytoplankton and periphyton also often exhibited reciprocal responses to physico-chemical parameters, with elevated (reduced) abundance of suspended (attached) communities in association with discharge, turbidity, and to a lesser extent dissolved N, while phytoplankton (periphyton) densities declined (increased) with dissolved N concentrations. GAMs of all biomarkers together revealed that the global responses of phototrophs to many environmental features reflected more pronounced influence of siliceous algae and chlorophytes (Fig. 6), possibly reflecting their preference for NO_3^- (Glibert et al. 2016; Swarbrick et al. 2019, Solomon et al. 2019). Taken together, these analyses confirm that small prairie streams exhibit abundant planktonic assemblages through much of the ice-free season (Wu et al. 2011; Breuer et al. 2016a), but that influx of NO_3^--rich, transparent urban effluent can

shift streams to biofilm-rich conditions more characteristic of forested (Vannote et al. 1980; Soininen et al. 2004; Dodds et al. 2002, 2006) or restored ecosystems (Riley and Dodds 2012), despite N limitation of phytoplankton (Supporting Information Fig. S1).

Phototroph abundance and composition in prairie streams

Elevated densities of diverse phytoplankton groups were recorded in both first-order headwaters and larger downstream reaches (Figs. 3, 4; Supporting Information Fig. S5). In contrast to the River Continuum Concept (Vannote et al. 1980), but similar to more recent studies of small eutrophic streams (Wu et al. 2011; Breuer et al. 2017), phytoplankton were abundant in these low-order ecosystems, with Chl a concentrations (up to 300 µg Chl a L^{-1}) generally greater than those recorded in large productive systems, such as the Dongjiang (Shimi et al. 2015), Thames (Moorhouse et al. 2018), Tigris (Varol and Şen 2018), Rhine, and Elbe rivers (Hardenbicker et al. 2014). Instead, suspended Chl a levels were comparable to values observed previously in regional lakes and rivers (Davies 2006; Pham et al. 2008; Waiser et al. 2011; Vogt et al. 2018) and were consistent with measurements in other nutrient-rich and agriculturally-influenced U.S and German temperate streams (Van Nieuwenhuyse and Jones 1996; Wu et al. 2011; Breuer et al. 2017). However, while regional eutrophic lakes that drain into the QR (Wascana, Buffalo Pound, Last Mountain; Fig. 1) principally support planktonic cyanobacteria (Vogt et al. 2018), including N_2-fixing forms (Donald et al. 2011; Hayes et al. 2019; Swarbrick et al. 2019), these small fluvial systems exhibited a predominance of siliceous algae (Fig. 4), mainly diatoms (Supporting Information Fig. 6), and some chlorophytes as seen in other larger rivers (Wehr and Descy 1998).

Despite abundant phytoplankton, periphyton were well developed in shallow marginal waters throughout the study system (Figs. 3, 4; Supporting Information Fig. S5). These benthic

phototrophs respond rapidly to nutrient fertilization (Dodds and Smith 2017) and indicate environmental degradation when Chl a exceeds 10 - 15 µg cm^{-2} (Welch et al. 1988) and filamentous cyanobacteria are common (Peterson and Grimm 1992; Murdock et al. 2004; McCall et al. 2017). Epilithic communities in this study deviated from these expectations in two significant ways. First, while colonial cyanobacteria were common in attached communities in headwaters and the QR reaches, particularly during late summer (Fig. 2.4; Supporting Information Fig. S5), associated Chl a values rarely exceeded 10 µg Chl a cm^{-2} at these locations (Fig. 3). Second, extremely high abundance of epilithon (15 – 30 µg Chl a cm^{-2}) in the effluent-influenced reaches of WC were composed mainly of diatoms and secondarily chlorophytes rather than colonial cyanobacteria (Fig. 4; Supporting Information Fig. S5). This pattern is similar that of Chételat et al. (1996) in which periphytic cyanobacteria occur in forested headwater streams, whereas urban eutrophic streams promote diatoms and chlorophytes, particularly nuisance *Cladophora* (Biggs and Price 1987; Dodds 1991; Hamdhani et al. 2020). In general, benthic Chl a levels were comparable to those seen in restored prairie streams (Riley and Dodds 2012), where may periphyton effectively capture and retain nutrients from flowing waters (Schiller et al. 2007, Smucker et al. 2014). Ironically, fatty-acid-rich epilithic diatoms normally indicate healthy aquatic ecosystems (Kelly and Whitton 1995; Stevenson et al. 2009; Lobo et al. 2016), with abundant secondary production (Feminella and Hawkins 1995); however, pollution-tolerant diatoms (Teittinen et al. 2015), particularly *Didymosphenia geminata* (Jackson et al. 2016), challenge that paradigm. Taken together, these observations suggest that effluent treated by BNR may reduce the symptoms of eutrophication in some N-limited lotic ecosystems by promoting diatom-rich biofilms over colonial cyanobacteria (Supporting Information Fig. S5),

despite addition of growth-saturating concentrations of N and P (Supporting Information Fig. S1).

Seasonality of primary producers

GAM analysis of Chl a demonstrated that phytoplankton, periphyton, and their ratio (Fig. 3), as well as many of more taxonomically-diagnostic biomarkers (Fig. 4; Supporting Information Fig. S5), exhibited significant seasonality in both years. However, seasonal development of suspended and epilithic phototrophs were generally opposite to each other in each year, with phytoplankton (periphyton) exhibiting spring maxima (minima) in 2018 and minima (maxima) in 2019 respectively. We infer that these patterns arise, in part, due to seasonal changes in lotic flow (Biggs and Close 1983; Dodds et al. 2004; Savoy et al. 2019), as marginal smooth effects of discharge on phototrophs were significant in GAMs (Fig. 5), opposite for suspended and attached assemblages (Fig 5), and demonstrated seasonal differences among years consistent with those observed for development of primary producers (Fig. 2) (Breuer et al. 2016). We infer that other physico-chemical parameters had less effect on the seasonality of phototrophs either because they had no significant unique effect on assemblages (temperature, TDN : SRP; but see below), their effects were not reciprocal in the two communities (Secchi depth, specific conductance, SRP), or because they exhibited limited or inconsistent seasonal variation (pH, most dissolved nutrients) (Stevenson and White 1995). However, while seasonal variation in abundance was noted for total phototrophs (Fig. 3), as well as some of the individual groups such as cyanobacteria (Fig. 4), the phenology of phytoplankton was not as strong or consistent as that seen in lakes regionally (McGowan et al. 2005; Swarbrick et al. 2019) and in other lotic ecosystems, where spring diatoms give way to summer chlorophytes and

cyanobacteria in suspended (Breuer et al. 2016; Moorhouse et al. 2018) and benthic habitats (Cattaneo et al. 1983; Peterson and Grimm 1992).

Phototroph phenology was partly obscured by influx of NO_3^--rich, transparent, urban wastewater to Wascana Creek (Figs. 3-6; Supporting Information Fig. S5). While previous studies report that WWTP effluent interferes with seasonal succession by promoting cyanobacteria (Davis et al. 1990; Murdock et al. 2004), herein wastewater sustained vernal siliceous algae (mainly diatoms; Supporting Information Fig. S5) and secondarily chlorophytes in phytoplankton (2018) and periphyton (2019), albeit not in the same year. Although speculative, we infer that differences among years in the habitat of spring diatom blooms within effluent-influenced reaches (see $\delta^{15}N$ in Fig. 2) may reflect the ability of periphyton to establish in spring (Biggs and Close 1983; Biggs 1996) due to high inter-annual variability in the proportion of flow derived from headwater discharge and wastewater sources, as well as the associated 'seeding' of planktonic assemblages from headwaters (Qu et al. 2019). For example, in May-June 2018, river flow in the urban-impacted reaches was derived equally from the WWTP and WC, whereas, in spring 2019 when periphyton abundance increased, less than 15% of flow was from headwaters (Supporting Information Fig. S6). Given that diatoms were the predominant group in the phytoplankton of WC (Fig. 4; Supporting Information Fig. S5), but not processed wastewater, variation in the relative contribution of headwater flow to total discharge may control the importance of headwater inocula and the magnitude of spring phytoplankton blooms.

Effects of WWTP discharge

Influx of urban effluent increased stream clarity and dissolved N content (Fig. 2) and was associated with a shift from phytoplankton to periphyton when recorded as trichromatic Chl a

(Fig. 3) or taxonomically-diagnostic pigments (Fig. 4; Supporting Information Fig. S5). These patterns reflected both declines in phytoplankton density (mainly 2018) and elevated abundance of epilithic diatoms and, secondarily, chlorophytes (2019). In particular, the reciprocal relationships between Secchi depth and phytoplankton (Fig. 5) as well as turbidity (not shown) suggests that high phytoplankton abundance was controlling the optical environment of the study streams, and that effluent diluted phytoplankton densities (see Supporting Information Fig. S7). Again, this effect appears most pronounced during 2018 when headwaters were more likely to provide suspended phototrophs into the WWTP-affected reach (Supporting Information Fig. S6). Because periphyton abundance was inversely and significantly related to phytoplankton (and turbidity), we infer that shading by suspended particles may have inhibited periphyton growth in headwaters and downstream reaches (Munn et al. 1989; Rosemond et al. 2000; Matthaei et al. 2010), similar to shading by riparian vegetation in forested streams (Munn et al. 2010; Julian et al. 2011), but that effluent may have alleviated light limitation. Similarly, although periphyton abundance was inversely related to Secchi depth (Figs. 5, 6), epilithon only declined at extremely high transparency, possibly because diatoms prefer low-light conditions (Litchman 2000) and may be photo-inhibited at high irradiance (Schwaderer et al. 2011; Glibert et al. 2016).

WWTP discharge also affected phytoplankton and periphyton assemblages by altering the nutrient regime within WC (Figs. 5, 6). Whereas upstream and QR phytoplankton exhibited growth limitation by N in microcosm experiments (Supporting Information Fig. S1) and both suspended and attached communities had abundant N_2-fixing cyanobacteria (Supporting Information Fig. S5), neither feature was common in effluent-impacted reaches of WC. Instead, phototrophic growth appeared saturated by elevated influx of NO_3^-, NH_4^+, and SRP, such as seen in other fertilized streams (Greene et al. 1975; Van Nieuwenhuyse and Jones 1996; Dodds et al.

2002, 2006) and consistent with the continuously elevated $\delta^{15}N$ values of phototrophs showing pronounced uptake of urban N in lower reaches of WC (Supporting Information Fig. S8; Leavitt et al. 2006). Instead of favouring cyanobacteria (Kim et al. 2020), alleviation of N limitation may have particularly favoured diatoms and chlorophytes (Figs. 4, 6), as seen in other NO_3^--rich systems (Breuer et al. 2017; Varol and Sen 2018; Solomon et al. 2019). Diatoms prefer NO_3^- because of their high nitrate reductase activity (Lomas and Glibert 2000), abundant NO_3^- transporters (Ambrust et al. 2004), and large intracellular NO_3^--storage vacuoles (Raven 1987; reviewed in Glibert et al. 2016), whereas chlorophytes tolerate and can be stimulated by high levels of both NO_3^- and NH_4^+ (Fernandez and Galvan 2007; Glibert et al. 2016; Bogard et al. 2020). In contrast, heterocystous cyanobacteria are often outcompeted in N-replete waters (Marcarelli et al. 2008; Caton et al. 2018; Bogard et al. 2020), while non-diazotrophic cyanobacteria prefer chemically-reduced N (NH_4^+, urea) over NO_3^- (Lee et al. 2015; Glibert et al. 2016) (Fig. 5). In general, inhibitory effects of NH_4^+ (Collos and Harrison 2014) may be limited in fluvial systems that are subject to high nutrient spiraling and rapid nitrification to NO_3^- (Peterson et al. 2001). Consistent with prior studies of regional eutrophic lakes, including Wascana (Swarbrick 2017), addition of dissolved P to already P-rich reaches (> 50 µg SRP L^{-1}) had little effect on phototrophic communities beyond a negative association with phytoplankton abundance (Fig. 5).

Effects of physico-chemical conditions in phototrophic assemblages

While growth of both lotic phytoplankton and periphyton often increases with water temperature (Baker and Baker 1979; Munn et al. 2002; Wu et al. 2011; Breuer et al. 2017), there was no significant effect of thermal regime on either assemblage in our study (GAM terms non-significant) despite a > 10 ^oC range in stream temperature (Fig. 2). However, as DOY effects

were significant in all GAMs, we infer that the unique effects of temperature may have been obscured by our temporal parameter. For example, although less pronounced than in some fluvial systems, algae and cyanobacteria followed a seasonal succession that was consistent with known temperature optima of phototrophic taxa (Sommer et al. 2012); spring diatoms and cryptophytes are cooler-water-adapted (17-22 °C), whereas chlorophytes (27-32 °C), and colonial cyanobacteria (27-37 °C) prefer higher temperatures seen in late summer (Fig. 2) (Paerl and Huisman 2008; Paerl2014; Visser et al. 2016). However, given that GAMs without DOY and distance only explained about 2% less for phytoplankton and 25% less deviance for periphyton than models that included temperature and DOY, we speculate that seasonal changes in water temperature played some role in phototrophic phenology, especially for phytoplankton (e.g., elevated cyanobacteria in August).

In addition to irradiance-mediated interactions between suspended and attached communities, phototrophic assemblages were also influenced by complex interactions among physico-chemical parameters (Figs. 5, 6). As seen elsewhere (Murdock et al. 2004), periphyton abundance decreased with discharge, particularly at higher velocities (>1 m s^{-1}) known to induce scouring of benthic habitats (Biggs 1995). In contrast, while phytoplankton are also expected to decline with discharge (Baker and Baker 1979; Leland 2003), turbulence-adapted planktonic taxa, such as diatoms and chlorophytes, tend to benefit from higher flow (Fig. 6) (Visser et al. 2016; but see Leland 2001) relative to positively-buoyant cyanobacteria (Guven and Howard 2006). Similarly, the slight, positive relationship of phytoplankton to pH in pigment-specific GAMs (Fig. 6) may reflect the fact the observation that both colonial cyanobacteria and pH were elevated in the QR and lakes that feed the river (Swarbrick 2017; Swarbrick et al. 2019).

748 In general, this study supported the hypotheses of Munn et al. (2002) and Black et al.
749 (2011) that local regulatory mechanisms can be overwhelmed by large anthropogenic processes,
750 as well as imposition of controls which operate at the landscape scale. Thus, while mechanisms
751 regulating primary producers in headwaters appeared to have been supressed by the influx of
752 urban effluent (see above) resulting in periphyton-rich streams characteristic of boreal habitats
753 (Vannote et al. 1980; Soinenen 2004; Thomas et al. 2015) or restored conditions (Riley and
754 Dodds 2012), these effects were themselves transitory, and eutrophic phytoplankton-rich
755 conditions were re-established downstream of the WC-QR confluence.

756 **2.5 Conclusions**

757 Global population growth has increased both nutrient pollution and atmospheric
758 warming, and is expected to exacerbate toxic cyanobacteria and degrade aquatic resources in the
759 next century (Carpenter et al. 1998; Schindler 2006; Dodds et al. 2009; Paerl and Paul 2012).
760 Scientific insights into the state of both lotic and lentic freshwaters is necessary to provide
761 policy-makers, stakeholders, and Indigenous communities with the ability to formulate effective
762 strategies to manage pollution and improve freshwater health (Leavitt et al. 2006; Dodds and
763 Smith 2017; Tank et al. 2018; Alexander et al. 2019). In particular, information is needed on
764 mechanisms to reduce harmful blooms in fluvial systems which are often more highly degraded
765 than standing waters (Birk et al. 2020)

766 In this study, influx of urban effluent resulted in an unexpected shift from phytoplankton
767 to periphyton, due to increased water clarity and NO_3^- fertilization. In particular, urban effluent
768 altered natural seasonality in both habitats, reduced colonial cyanobacteria in both habitats, and
769 favoured development of siliceous algae and chlorophytes due to multiple mechanisms (Sommer
770 et al. 2012; Breuer et al. 2016). Comparison between reaches also suggested that the dilution

771 effect of urban wastewater was limited to first-order streams and that normal patterns of seasonal
772 succession were re-established in phytoplankton-rich second-order systems (Munn et al. 2002;
773 Black et al. 2011; Andrus et al. 2013). Taken together, these patterns suggest that wastewater
774 treatment with BNR has clear environmental benefits (Holeton et al. 2011), resulting in a turbid,
775 phytoplankton-rich stream resembling a restored ecosystem characterized by diatom-rich
776 biofilms.

777 **Acknowledgements**

778 We thank members of the Limnology Laboratory for assistance with data collection since
779 2009. We also thank Curtis Hallborg and Trent Wurtz of the Saskatchewan Water Security
780 Agency for data on surface flow in the Qu'Appelle River drainage basin, as well as Kayla
781 Gallant and EPCOR for wastewater information and data, Drs. K. Hodder and V. Swarbrick for
782 assistance with discharge calculations, and Zora Quinones-Rivera and D. Bateson for HPLC
783 assistance. This work was supported by the NSERC Canada Discovery Grants program, Canada
784 Research Chairs, Canada Foundation for Innovation, the Province of Saskatchewan, the
785 University of Regina, and Queens University Belfast. We acknowledge that the study sites are
786 on Treaty 4 territory and appreciate the willingness of the Indigenous Peoples of Saskatchewan
787 to protect and share Canada's water resources. This is a contribution of the Qu'Appelle Valley
788 long-term ecological research program (QU-LTER).

References

Affourtit J., J. P. Zehr, and H. W. Paerl 2001. Distribution of nitrogen-fixing microorganisms along the Neuse River Estuary, North Carolina. Microb. Ecol. **41**:114–123. doi:10.1007/s002480000090

Agriculture and Agri-Food Canada. 2008. Watershed Boundaries of the Prairie Farm Rehabilitation Administration Project. Government of Canada.

Allan, J. D. 2004. Landscapes and riverscapes: The influence of land use on stream ecosystems. Annual Review of Ecology, Evolution, and Systematics **35**: 257–284. doi:10.1146/annurev.ecolsys.35.120202.110122

Andrus, M. J., and others. 2015. Spatial and temporal variation of algal assemblages in six Midwest agricultural streams having varying levels of atrazine and other physico-chemical attributes. Sci. Total Environ. **505**: 65–89. doi:10.1016/j.scitotenv.2014.09.033

APHA-AWWA/WEF. 1998. Standard Methods for the Examination of Water and Wastewater, 20th Edition. American Public Health Association, Washington DC, USA.

Armbrust, E. V., and others. 2004. The genome of the diatom *Thalassiosira pseudonana*: Ecology, evolution, and metabolism. Sci. **306**: 79–86. doi:10.1126/science. 1101156

Baker, A. L., and K. K. Baker. 1979. Effects of temperature and current discharge on the concentration and photosynthetic activity of the phytoplankton in the upper Mississippi River. Freshw. Biol. **9**: 191–198. doi:10.1111/j.1365-2427.1979.tb01502.x

Baker P. D., and A. R. Humpage. 1994. Toxicity associated with commonly occurring cyanobacteria in surface waters of the Murray-Darling Basin, Australia. Aust. J. Freshw. Res. **45**: 773–786. doi:10.1071/MF9940773

Bellinger, E. G., and D. C. Sigee. 2010. Sampling, Biomass Estimation and Counts of Freshwater Algae, p. 41-97. *In* Bellinger, E. G., and D. C. Sigee. [ed.], Freshwater Algae: Identification and Use as Bioindicators. John Wiley & Sons. doi:10.1002/9780470689554.ch2

Bernhardt, E. S., and others. 2017. The metabolic regimes of flowing waters. Limnol. Oceanogr. **63**: S99-S118. doi:10.1002/lno.10726

Biggs, B. J. F. 1995. The contribution of flood disturbance, catchment geology and land use to the habitat template of periphyton in stream ecosystems. Freshw. Biol. **33**: 419–438. doi:10.1111/j.1365-2427.1995.tb00404.x

Biggs, B. J. F. 1996. Patterns in Benthic Algae of Streams, p. 31-51. *In* Stevenson, R. J., M. L. Bothwell, and R. L. Lowe. [eds.], Algal Ecology. Freshwater Benthic Ecosystems. Academic Press.

Biggs, B. J. F. 2000. Eutrophication of streams and rivers: Dissolved nutrient-chlorophyll relationships for benthic algae. J. N. Am. Benthol. Soc. **19**: 17–31. doi:10.2307/1468279

Biggs, B. J. F., and M. E. Close. 1989. Periphyton biomass dynamics in gravel bed rivers: The relative effects of flow and nutrients. Freshw. Biol. **22:** 209–231.

Biggs, B. J. F., and Price, G.M. 1987. A survey of filamentous algal proliferations in New Zealand rivers. N.Z. J. Mar. Freshw. Res. **21**: 175–191.

Birk, S., and others. 2020. Impacts of multiple stressors on freshwater biota across spatial scales and ecosystems. Nat. Ecol. Evol. doi:10.1038/s41559-020-1216-4

Black, R. W., P. W. Moran, and J. D. Frankforter. 2010. Response of algal metrics to nutrients and physical factors and identification of nutrient thresholds in agricultural streams. Environ. Monit. Assess. **175**: 397–417. doi:10.1007/s10661-010-1539-8

Bogard, M. J., D. B. Donald, K. Finlay, and P. R. Leavitt. 2012. Distribution and regulation of urea in lakes of central North America. Freshw. Biol. **57**: 1277-1292. doi.org/10.1111/j.1365-2427.2012.02775.x

Bogard, M. J., R. J. Vogt, N. M. Hayes, and P. R. Leavitt. 2020. Unabated nitrogen pollution favours growth of toxic cyanobacteria over chlorophytes in most hypereutrophic lakes. Environ. Sci. Technol. **54:** 3219–3227. doi.org/10.1021/acs.est.9b06299

Breuer, F., P. Janz, E. Farrelly, and K. P. Ebke. 2016. Seasonality of algal communities in small streams and ditches in temperate regions using delayed fluorescence. J. Freshw. Ecol. **31**: 393-406, DOI:10.1080/02705060.2016.1160846

Breuer, F., P. Janz, E. Farrelly, and K.-P. Ebke. 2017. Environmental and structural factors influencing algal communities in small streams and ditches in central Germany. J. Freshw. Ecol. **32**: 65-83. doi:10.1080/02705060.2016.1241954

Buchanan, T. J., and W. P. Somers. 1976. Discharge Measurements at Gauging Stations, p. 1-65. *In* U.S. Geological Survey [eds.], Techniques of Water-Resources Investigations of the United States Geological Survey - Book 3: Applications of Hydraulics. United States Government Printing Office.

Bürkner, P. 2018. Advanced Bayesian Multilevel Modeling with the R Package brms. R J. **10**: 395–411. doi:10.32614/RJ-2018-017.

Burliga, A. L., and J. P. Kociolek. 2016. Diatoms (Bacillariophyta) in Rivers, p. 93-128. *In* O. Necchi JR [ed.], River Algae. Springer. doi:10.1007/978-3-319-31984-1_11

Carey, R. O., and K. W. Migliaccio. 2009. Contribution of wastewater treatment plant effluents to nutrient dynamics in aquatic systems: a review. Environ. Manage. **44**: 205–17. doi:10.1007/s00267-009-9309-5

Carpenter, S. R., N. F. Caraco, D. L. Correll, R. W. Howarth, A. N. Sharpley, and V. H. Smith. 1998. Nonpoint pollution of surface waters with phosphorus and nitrogen. Ecol. Appl. **8**: 559–568. doi:10.1890/1051-0761(1998)008[0559:nposww]2.0.co;2

Casamatta, D. A., and P. Hašler. 2016. Blue-Green Algae (Cyanobacteria) in Rivers, p. 5-34. *In* O. Necchi JR [ed.], River Algae. Springer. doi:10.1007/978-3-319-31984-1_11

Cattaneo, A. 1983. Grazing epiphytes. Limnol. Oceanog. **28:** 124– 132.

Cattaneo, A., and M. C. Amireault. 1992. How artificial are artificial substrata for periphyton? J. N. Am. Benthol. Soc. **11**: 244–256. doi:10.2307/1467389

Caton, I. R., T. M. Caton, and M. A. Schneegurt. 2018. Nitrogen-fixation activity and the abundance and taxonomy of nifH genes in agricultural, pristine, and urban prairie stream sediments chronically exposed to different levels of nitrogen loading. Arch. Microbiol. doi:10.1007/s00203-018-1475-5

Chambers, P. A., D. J. McGoldrick, R. B. Brua, C. Vis, J. M. Culp, and G. A. Benoy. 2012. Development of environmental thresholds for nitrogen and phosphorus in streams. J. Environ. Qual. **41**: 7-20 doi:10.2134/jeq2010.0273

Chételat, J., F. R. Pick, A. Morin, and P. B. Hamilton. 1999. Periphyton biomass and community composition in rivers of different nutrient status. Can. J. Fish. Aquat. Sci **56**: 560–569. doi:10.1139/f98-197

Collos, Y., and P. J. Harrison. 2014. Acclimation and toxicity of high ammonium concentrations to unicellular algae. Mar. Pollut. Bull. **80**: 8–23. doi:10.1016/j.marpolbul.2014.01.006

Davies J- M. 2006. Application of the Canadian Water Quality Index for assessing changes in water quality along the Qu'Appelle River, Saskatchewan, Canada. Lake and Reservoir Manag. **22**: 308-320. doi:10.1080/07438140609354365.

Davis, L. S., Hoffman, J. P., and P. W. Cook. 1990. Seasonal succession of algal periphyton from a wastewater treatment facility. J. Phycol. **26**: 611–617.

Dodds, W.K. 1991. Factors associated with dominance of the filamentous green alga *Cladophora glomerata*. Water Res. **25**: 1325–1332.

Dodds, W. K. 2007. Trophic state, eutrophication and nutrient criteria in streams. Trends Ecol. Evol. **22**: 669–676. doi:10.1016/j.tree.2007.07.010

Dodds, W. K., W. W. Bouska, J. L. Eitzmann, T. J. Pilger, K. L. Pitts, A. J. Riley, J. T. Schloesser, and D. J. Thornbrugh. 2009. Eutrophication of U.S. Freshwaters: Analysis of Potential Economic Damages. Environ. Sci. and Technol. **43**: 12–19. doi:10.1021/es801217q

Dodds, W. K., and V. H. Smith. 2017. Nitrogen, phosphorus, and eutrophication in streams. Inland Wat. **6**: 155–164. doi:10.5268/IW-6.2.909

Dodds, W. K., V. H. Smith, and K. Lohman. 2002. Nitrogen and phosphorus relationships to benthic algal biomass in temperate streams. Can. J. Fish. Aquat. Sci. **59**: 865–874.

Dodds, W. K., V. H. Smith, and K. Lohman. 2006. Nitrogen and phosphorus relationships to benthic algal biomass in temperate streams. Can. J. Fish. Aquat. Sci. **63**: 1190–1191.

Donald, D. B., M. J. Bogard, K. Finlay, and P. R. Leavitt. 2011. Comparative effects of urea, ammonium, and nitrate on phytoplankton abundance, community composition, and toxicity in hypereutrophic freshwaters. Limnol. Oceanogr. **56**: 2161–2175. doi:10.4319/lo.2011.56.6.2161

Dylla, N. P., 2019. Downstream effects on denitrification and nitrous oxide from an advanced wastewater treatment plant upgrade. MSc thesis. University of Saskatchewan, Saskatoon, Canada. 124 pp.

Feminella, J. W., and C. P. Hawkins. 1995. Interactions between stream herbivores and periphyton: A quantitative analysis of past experiments. J. N. Am. Benthol. Soc. **14**: 465–509. doi:10.2307/1467536

Fernandez, E., and A. Galvan. 2007. Inorganic nitrogen assimilation in Chlamydomonas. J. Exp. Bot. **58**: 2279–2287. doi:10.1093/jxb/erm106

Filoso, S., and M. A. Palmer. 2011. Assessing stream restoration effectiveness at reducing nitrogen export to downstream waters. Ecol. Appl. **21**: 1989–2006. doi:10.1890/10-0854.1

Gianfagna, C. C., C. E. Johnson, D. G. Chandler, and C. Hofmann. 2015. Watershed area ratio accurately predicts daily streamflow in nested catchments in the Catskills, New York. J. Hydrol. Reg. Stud. **4**: 583-594. doi:10.1016/j.ejrh.2015.09.002

Giller, P., and B. Malmqvist. 1998. The Biology of Streams and Rivers. Biology of Habitats. Oxford University Press.

Glibert, P. M., and others. 2016. Pluses and minuses of ammonium and nitrate uptake and assimilation by phytoplankton and implications for productivity and community composition, with emphasis on nitrogen-enriched conditions. Limnol. Oceanogr. **61**: 165–197. doi:10.1002/lno.10203

Greene, J. C., W. E. Miller, T. Shiroyama, and T. E. Maloney. 1975. Utilization of algal assays to assess the effects of municipal, industrial, and agricultural wastewater effluents upon phytoplankton production in the Snake River system. Water. Air. Soil Pollut. **4**: 415–434. doi:10.1007/bf00280726

Grimm, N. B., S. H. Faeth, N. E. Golubiewski, C. L. Redman, J. Wu, X. Bai, and J. M. Briggs. 2008. Global change and the ecology of cities. Science **319**: 756–760. doi:10.1126/science.1150195

Guildford, S. J., and R. E. Hecky. 2000. Total nitrogen, total phosphorus, and nutrient limitation in lakes and oceans: Is there a common relationship? Limnol. Oceanogr. **45**: 1213–1223. doi:10.4319/lo.2000.45.6.1213

Guven, B., and A. Howard. 2006. Modelling the growth and movement of cyanobacteria in river systems. Sci. Total Environ. **368**: 898–908. doi:10.1016/j.scitotenv.2006.03.035

Haig, H. A., N. M. Hayes, G. L. Simpson, Y. Yi, B. Wissel, K. R. Hodder, and P. R. Leavitt. 2020. Comparison of isotopic mass balance and instrumental techniques as estimates of basin hydrology in seven connected lakes over 12 years. J. Hydrol. X **6**: 100046. doi.org/10.1016/ j.hydroa.2019.100046

Hall, R. I., P. R. Leavitt, R. Quinlan, A. S. Dixit, and J. P. Smol. 1999. Effects of agriculture, urbanization and climate on water quality in the northern Great Plains. Limnol. Oceanogr. **43**: 739–756.

Hamdhani, H., D. E. Eppehimer, and M. T. Bogan. 2020. Release of treated effluent into streams: A global review of ecological impacts with a consideration of its potential use for environmental flows. Freshwater. Biol. doi:10.1111/fwb.13519

941 Hardenbicker, P., S. Rolinski, M. Weitere, and H. Fischer. 2014. Contrasting long-term trends
942 and shifts in phytoplankton dynamics in two large rivers. Int. Rev. Hydrobiol. **99**: 287–
943 299. doi:10.1002/iroh.201301680
944 Hayes, N. M., A. Patoine, H. A. Haig, G. L. Simpson, V. J. Swarbrick, E. Wiik, and P. R.
945 Leavitt. 2019. Spatial and temporal variation in nitrogen fixation and its importance to
946 phytoplankton in phosphorus-rich lakes. Freshw. Biol. **64**: 269–283.
947 doi:10.1111/fwb.13214
948 Holeton, C., P. A. Chambers, L. Grace, and K. Kidd. 2011. Wastewater release and its impacts
949 on Canadian waters. Can. J. Fish. Aquat. Sci. **68**: 1836–1859. doi:10.1139/f2011-096
950 Hutchins, M. G., A. C. Johnson, A. Deflandre-Vlandas, S. Comber, P. Posen, and D. Boorman.
951 2010. Which offers more scope to suppress river phytoplankton blooms: Reducing nutrient
952 pollution or riparian shading? Sci. Total Environ. **408**: 5065–5077.
953 doi:10.1016/j.scitotenv.2010.07.033
954 Jackson, L. J., L. Corbett, and G. Scrimgeour. 2016. Environmental constraints on
955 Didymosphenia geminata occurrence and bloom formation in Canadian Rocky Mountain
956 lotic systems. Can. J. Fish. Aquat. Sci. **73**: 964–972. doi:10.1139/cjfas-2015-0361
957 Jeffrey, S. W., and G. F. Humphrey. 1975. New spectrophotometric equations for determining
958 chlorophylls a, b, c1 and c2 in higher plants, algae and natural phytoplankton. Biochem.
959 Physiol. Pfl. **167**: 191–194. doi:10.1016/s0015-3796(17)30778-3
960 Julian, J. P., S. Z. Seegert, S. M. Powers, E. H. Stanley, and M. W. Doyle. 2011. Light as a first-
961 order control on ecosystem structure in a temperate stream. Ecohydrology **4**: 422–432.
962 doi:10.1002/eco.144
963 Kelly, M. G., and B. A. Whitton. 1995. The Trophic Diatom Index: a new index for monitoring
964 eutrophication in rivers. J. Appl. Phycol. **7**: 433–444. doi:10.1007/BF00003802
965 Kim, K., and others. 2020. Nitrogen stimulates *Microcystis*-dominated blooms more than
966 phosphorus in river conditions that favor non-nitrogen-fixing genera. Environ. Sci.
967 Technol. **54**: 7185–7193. doi:10.1021/acs.est.9b07528
968 Klausmeier, C. A., E. Litchman, T. Daufresne, and S. A. Levin. 2004. Optimal nitrogen-to-
969 phosphorus stoichiometry of phytoplankton. Nature **429**: 171-174.
970 doi:10.1038/nature02454

971 Lamberti, G. A. 1996. The Role of Periphyton in Benthic Food Webs, p. 533–572. *In* Stevenson,
972 R. J., M. L. Bothwell, and R. L. Lowe. [eds.], Algal Ecology. Freshwater Benthic
973 Ecosystems. Academic Press.
974 Leavitt, P. R. 1993. A review of factors that regulate carotenoid and chlorophyll deposition and
975 fossil pigment abundance. J. Paleolimnol. **9**: 109-127. doi:10.1007/BF00677513
976 Leavitt, P. R., and D. A. Hodgson. 2001. Sedimentary pigments, p. 295-325. *In* J. P. Smol, H. J.
977 B. Birks, and W. M. Last (eds.), Tracking Environmental Change using Lake Sediments.
978 Volume 3: Terrestrial, Algal and Siliceous Indicators. Kluwer. doi:10.1007/0-306-47668-
979 1_15
980 Leavitt, P. R., C. S. Brock, C. Ebel, and A. Patoine. 2006. Landscape-scale effects of urban
981 nitrogen on a chain of freshwater lakes in central North America. Limnol. Oceanogr. **51**:
982 2262–2277. doi:10.4319/lo.2006.51.5.2262
983 Lee, J., A. E. Parker, F. P. Wilkerson, and R. C. Dugdale. 2015. Uptake and inhibition kinetics of
984 nitrogen in Microcystis aeruginosa: Results from cultures and field assemblages collected
985 in the San Francisco Bay Delta, CA. Harmful Algae **47**: 126–140.
986 doi:10.1016/j.hal.2015.06.002
987 Leland, H. V. 2003. The influence of water depth and flow regime on phytoplankton biomass
988 and community structure in a shallow, lowland river. Hydrobiologia **506–509**: 247–255.
989 doi:10.1023/b:hydr.0000008596.00382.56
990 Leland, H. V., L. R. Brown, and D. K. Mueller. 2001. Distribution of algae in the San Joaquin
991 River, California, in relation to nutrient supply, salinity and other environmental factors.
992 Freshw. Biol. **46**: 1139–1167. doi:10.1046/j.1365-2427.2001.00740.x
993 Litchman, E. 2000. Growth rates of phytoplankton under fluctuating light. Freshw. Biol. **44**:
994 223–235. doi:10.1046/j.1365-2427.2000.00559.x
995 Lobo, E. A., C. G. Heinrich, M. Schuch, C. E. Wetzel, and L. Ector. 2016. Diatoms as
996 Bioindicators in Rivers, p. 245-271. *In* O. Necchi JR [ed.], River Algae. Springer.
997 doi:10.1007/978-3-319-31984-1_11
998 Lomas, M. W., and P. M. Glibert. 2000. Comparisons of nitrate uptake, storage and reduction in
999 marine diatoms and flagellates. J. Phycol. **36**: 903–913.

Loza, V., E. Perona, and P. Mateo. 2012. Molecular fingerprinting of cyanobacteria from river biofilms as a water quality monitoring tool. Appl. Environ. Microb. **79**: 1459–72. doi:10.1128/aem.03351-12

Lu, H., Y. Feng, J. Wang, Y. Wu, H. Shao, and L. Yang. 2016. Responses of periphyton morphology, structure, and function to extreme nutrient loading. Environ. Pollut. **214**: 878–84. doi:10.1016/j.envpol.2016.03.069

Marcarelli, A. M., M. A. Baker, and W. A. Wurtsbaugh. 2008. Is in-stream N_2 fixation an important N source for benthic communities and stream ecosystems? J. N. Am. Benthol. Soc. **27**: 186–211. doi:10.1899/07-027.1

Marra, G., and S. N. Wood. 2011. Practical variable selection for generalized additive models. Comput. Stat. Data. An. **55**: 2372–2387. doi:10.1016/j.csda.2011.02.004

Matthaei, C. D., J. J. Piggott, and C. R. Townsend. 2010. Multiple stressors in agricultural streams: interactions among sediment addition, nutrient enrichment and water abstraction: Sediment, nutrients & water abstraction. J. Appl. Ecol. **47**: 639–649. doi:10.1111/j.1365-2664.2010.01809.x

McGowan, S., A. Patoine, M. D. Graham, and P. R. Leavitt. 2005. Intrinsic and extrinsic controls on lake phytoplankton synchrony as illustrated by algal pigments. Verh. Internat. Verein. Limnol. **29**: 794-798. doi:10.1080/03680770.2005.11902787

McCall, S. J., M. S. Hale, J. T. Smith, D. S. Read, and M. J. Bowes. 2017. Impacts of phosphorus concentration and light intensity on river periphyton biomass and community structure. Hydrobiologia **792**: 315–330. doi:10.1007/s10750-016-3067-1

Mischke, U., M. Venohr, and H. Behrendt. 2011. Using phytoplankton to assess the trophic status of German rivers. Int. Rev. of Hydrobiol. **96**: 578–598. doi:10.1002/iroh.201111304

Moorhouse, H. L., and others. 2018. Characterisation of a major phytoplankton bloom in the River Thames (UK) using flow cytometry and high performance liquid chromatography. Sci. Total Environ. **624**: 366–376. doi:10.1016/j.scitotenv.2017.12.128

Morin, A., and A. Cattaneo. 1992. Factors affecting sampling variability of freshwater periphyton and the power of periphyton studies. Can. J. Fish. Aquat. Sci. **49**: 1695– 1703

Mowchenko, M., and P. O. Meid. 1983. The determination of gross and effective drainage areas in the Prairie Provinces. Hydrology report #104. Prairie Farm Rehabilitation Administration, Engineering Branch, Regina, Saskatchewan.

1031 Munn, M. D., R. W. Black, and S. J. Gruber. 2002. Response of benthic algae to environmental
1032 gradients in an agriculturally dominated landscape. J. N. Am. Benthol. Soc. **21**: 221–237.
1033 doi:10.2307/1468411
1034 Munn, M., J. Frey, and A. Tesoriero. 2010. The influence of nutrients and physical habitat in
1035 regulating algal biomass in agricultural streams. Environ. Manage. **45**: 603–15.
1036 doi:10.1007/s00267-010-9435-0
1037 Munn, M. D., L. L. Osborne, and M. J. Wiley. 1989. Factors influencing periphyton growth in
1038 agricultural streams of central Illinois. Hydrobiologia **174**: 89–97. doi:10.1007/bf00014057
1039 Murdock, J., D. Roelke, and F. Gelwick. 2004. Interactions between flow, periphyton, and
1040 nutrients in a heavily impacted urban stream: implications for stream restoration
1041 effectiveness. Ecol. Eng. **22**: 197–207. doi:10.1016/j.ecoleng.2004.05.005
1042 Natural Resources Canada. 2016. CanVec. https://www.nrcan.gc.ca/science-and-data/science-
1043 and-research/earth-sciences/geography/topographic-information/download-directory-
1044 documentation/17215.
1045 Oksanen, J., and others. 2019. 'Vegan' Community Ecology. https://cran.r-
1046 project.org/web/packages/vegan/vegan.pdf
1047 Paerl, H.W. 2014. Mitigating harmful cyanobacterial blooms in a human- and climatically-
1048 impacted world. Life **4**: 988–1012. doi:10.3390/life4040988
1049 Paerl, H. W., and J. Huisman. 2008. Climate: Blooms like it hot. Science **320**: 57–58.
1050 doi:10.1126/science.1155398
1051 Paerl, H. W., and T. G. Otten. 2013. Harmful cyanobacterial blooms: Causes, consequences, and
1052 controls. Microb. Ecol. **65**: 995–1010. doi:10.1007/s00248-012-0159-
1053 Paerl, H. W., and V. J. Paul. 2012. Climate change: Links to global expansion of harmful
1054 cyanobacteria. Water Res. **46**: 1349–1363. doi:10.1016/j.watres.2011.08.002.
1055 Patoine, A., and P. R. Leavitt. 2006. Century-long synchrony of fossil algae in a chain of
1056 Canadian Prairie Lakes. Ecology **87**: 1710–1721. doi:10.1890/0012-
1057 9658(2006)87[1710:CSOFAI]2.0.CO;2
1058 Paul, M. J., and J. L. Meyer. 2001. Streams in the Urban Landscape. Annu. Rev. Ecol. Evol.
1059 Syst. **32**: 333–365. doi:10.1146/annurev.ecolsys.32.081501.114040

Pedersen, E. J., D. L. Miller, G. L. Simpson, and N. Ross. 2019. Hierarchical generalized additive models in ecology: An introduction with mgcv. Peerj. **7**: e6876. doi:10.7717/peerj.6876

Peterson, C.G., and N. B. Grimm. 1992. Temporal variation in enrichment effects during periphyton succession in a nitrogen limited desert stream ecosystem. J. N. Am. Benthol. Soc. **11**: 20–36.

Peterson, B. J., and others. 2001. Control of nitrogen export from watersheds by headwater streams. Science **292**: 86–90. doi:10.1126/science.1056874

Pham, S. V., P. R. Leavitt, S. McGowan, and P. Peres-Neto. 2008. Spatial variability of climate and land use effects on lakes of the northern Great Plains. Limnol. Oceanogr. **53**: 728-742. doi.org/10.4319/lo.2008.53.2.0728

Pham, S. V., P. R. Leavitt, S. McGowan, B. Wissel, and L. I. Wassenaar. 2009. Spatial and temporal variability of prairie lake hydrology as revealed using stable isotopes of hydrogen and oxygen. Limnol. Oceanogr. **54**: 101–118. doi:10.4319/lo.2009.54.1.0101

Pomeroy, J. W., D. M. Gray, T. Brown, N. R. Hedstrom, W. L. Quinton, R. J. Granger, and S. K. Carey. 2007. The cold regions hydrological model: A platform for basing process representation and model structure on physical evidence. Hydrol. Process. **21**: 2650-2667. doi.org/10.4319/lo.2009.54.1.0101

Qu, Y., N. Wu, B. Guse, and N. Fohrer. 2018. Riverine phytoplankton shifting along a lentic-lotic continuum under hydrological, physiochemical conditions and species dispersal. Sci. Total Environ. **619-620**: 1628-1636. doi:10.1016/j.scitotenv.2017.10.139

R Core Team. 2018. R: a language and environment for statistical computing; https://www.R-project.org/

Raven, J. A. 1987. The role of vacuoles. New Phytol. **106**: 357–422. doi:10.1083/jcb.104.2.3634

Rahm, B.G., Hill, N.B., Shaw, S.B., Riha, S.J., 2016. Nitrate dynamics in two streams impacted by wastewater treatment plant discharge: point sources or sinks? J. Am. Water Resour. Assoc. **52**: 592–604.

Reynolds, C. S. 1988. Potamoplankton: paradigms, paradoxes, prognoses. *In* Round, F. E. [ed.], p. 285–311, Algae and the Aquatic Environment. Biopress Ltd., Bristol.

Reynolds, C. S. 1994. The long, the short and the stalled: on the attributes of phytoplankton selected by physical mixing in lakes and rivers. Hydrobiologia **289**: 9–21. doi:10.1007/bf00007405

Reynolds, C. S., and J. -P. Descy. 1996. The production, biomass and structure of phytoplankton in large rivers. River Systems **10**: 161–187. doi:10.1127/lr/10/1996/161

Riley, A. J., and W. K. Dodds. 2012. The expansion of woody riparian vegetation, and subsequent stream restoration, influences the metabolism of prairie streams. Freshw. Biol. **57**: 1138–1150. doi:10.1111/j.1365-2427.2012.02778.x

Roeder, D. R. 1977. Relationships between phytoplankton and periphyton communities in a central Iowa stream. Hydrobiologia **56**: 145–151. doi:10.1007/bf00023353

Rosemond, A. D., P. J. Mulholland, and S. H. Brawley. 2000. Seasonally shifting limitation of stream periphyton: response of algal populations and assemblage biomass and productivity to variation in light, nutrients, and herbivores. Can. J. Fish. Aquat. Sci. **57**: 66–75. doi:10.1139/f99-181

Savoy, P., A. P. Appling, J. B. Heffernan, E. G. Stets, J. S. Read, J. W. Harvey, and E. S. Bernhardt. 2019. Metabolic rhythms in flowing waters: An approach for classifying river productivity regimes. Limnol. Oceanogr. **64**: 1835-1851. doi:10.1002/lno.11154

Schiller, D. V., E. Martí, J. L. Riera, and F. Sabater. 2007. Effects of nutrients and light on periphyton biomass and nitrogen uptake in Mediterranean streams with contrasting land uses. Freshw. Biol. **52**: 891–906. doi:10.1111/j.1365-2427.2007.01742.x

Schindler, D. W. 2006. Recent advances in the understanding and management of eutrophication. Limnol. Oceanogr. **51**: 356–363. doi:10.4319/lo.2006.51.1_part_2.0356

Schwaderer, A. S., K. Yoshiyama, P. de T. Pinto, N. G. Swenson, C. A. Klausmeier, and E. Litchman. 2011. Eco-evolutionary differences in light utilization traits and distributions of freshwater phytoplankton. Limnol. Oceanogr. **56**: 589–598. doi:10.4319/lo.2011.56.2.0589

Scott, T. J., and M. J. McCarthy. 2010. Nitrogen fixation may not balance the nitrogen pool in lakes over timescales relevant to eutrophication management. Limnol. Oceanogr. **55**: 1265–1270. doi:10.4319/lo.2010.55.3.1265

Scott, J. T., and A. M. Marcarelli. 2012. Cyanobacteria in Freshwater Benthic Environments, p. 271-289. *In* B.A. Whitton (ed.), Ecology of Cyanobacteria II. doi:10.1007/978-94-007-3855-3_9

Sherwood, A.R. 2016. Green Algae (Chlorophyta and Streptophyta) in Rivers, p. 35-63. *In* O. Necchi JR [ed.], River Algae. Springer. doi:10.1007/978-3-319-31984-1_11

Shimi, T., Y. Yang, Q. Yongmin, H. Wenxiang, L. Jianhua, W. Dongyu, and C. P. of Hydrobiology. 2015. Temporal and spatial distribution of phytoplankton chlorophyll-a and its relationships with environmental factors in Dongjiang River, Pearl River basin. J. Lake Sci. **27**: 31–37. doi:10.18307/2015.0104

Smucker, N. J., S. A. Drerup, and M. L. Vis. 2014. Roles of benthic algae in the structure, function, and assessment of stream ecosystems affected by acid mine drainage. J. Phycol. **50**: 425–436. doi:10.1111/jpy.12184

Soininen, J., R. Paavola, and T. Muotka. 2004. Benthic diatom communities in boreal streams: community structure in relation to environmental and spatial gradients. Ecography **27**: 330–342. doi:10.1111/j.0906-7590.2004.03749.x

Solomon, C. M., M. Jackson, and P. M. Glibert. 2019. Chesapeake Bay's "forgotten" Anacostia River: eutrophication and nutrient reduction measures. Environ. Monit. Assess. **191**: 265. doi:10.1007/s10661-019-7437-9

Sommer, U., R. Adrian, L. Domis, and others. 2012. Beyond the Plankton Ecology Group (PEG) model: Mechanisms driving plankton succession. Annu. Rev. Ecol. Evol. Syst. **43**: 429–448. doi:10.1146/annurev-ecolsys-110411-160251

Steinman, A. D., G. A. Lamberti, P. R. Leavitt, and D. G. Uzarski. 2017. Biomass and Pigments of Benthic Algae, p. 223-241. *In* Hauer, F.R., and G. A. Lamberti [eds.], Methods in Stream Ecology, Volume 1. Academic press. doi:10.1016/b978-0-12-416558-8.00012-3

Stevenson, R. J. 1997. Scale-Dependent Determinants and Consequences of Benthic Algal Heterogeneity. J. N. Am. Benthol. Soc. **16**: 248–262. doi:10.2307/1468255

Stevenson, R. J., and K. D. White. 1995. A comparison of natural and human determinants of phytoplankton communities in the Kentucky River basin, USA. Hydrobiologia **297**: 201–216. doi:10.1007/bf00019285

Stevenson, R. J., Y. Pan, and H. van Dam. 2009. Assessing environmental conditions in rivers and streams with diatoms, p. 57-85. *In* Smol, J.P., and E. F. Stoermer [eds.], The Diatoms. Cambridge University Press. doi:10.1017/cbo9780511763175.005

1149 Swarbrick, V. J. 2017. Season impacts and regulation of nitrogen pollutions in the Northern
1150 Great Plains: Insights from microcosm, mesocosm, and mensurative-scale studies. PhD
1151 thesis. University of Regina. 217 pp.
1152 Swarbrick, V. J., G. L. Simpson, P. M. Glibert, and P. R. Leavitt. 2019. Differential stimulation
1153 and suppression of phytoplankton growth by ammonium enrichment in eutrophic
1154 hardwater lakes over 16 years. Limnol. Oceanogr. **64**: S130–S149. doi:10.1002/lno.11093
1155 Tank, J. L., and W. K. Dodds. 2003. Nutrient limitation of epilithic and epixylic biofilms in ten
1156 North American streams. Freshw. Biol. **48**: 1031–1049. doi:10.1046/j.1365-
1157 2427.2003.01067.x
1158 Tank, J. L., and others. 2018. Partitioning assimilatory nitrogen uptake in streams: An analysis of
1159 stable isotope tracer additions across continents. Ecol. Monogr. **88**: 120–138.
1160 doi:10.1002/ecm.1280
1161 Taranu, Z. E., and others. 2015. Acceleration of cyanobacterial dominance in north temperate-
1162 subarctic lakes during the Anthropocene. Ecol. Lett. **18**: 375–384. doi:10.1111/ele.12420
1163 Teittinen, A., M. Taka, O. Ruth, and J. Soininen. 2015. Variation in stream diatom communities
1164 in relation to water quality and catchment variables in a boreal, urbanized region. Sci. Total
1165 Environ. **530–531**: 279–89. doi:10.1016/j.scitotenv.2015.05.101
1166 Thomas, K E., R. I. Hall, and G. J. Scrimigeour. 2013. Evaluating the use of algal pigments to
1167 assess the biological condition of streams. Environ. Monit. Assess. **185**: 7895–7913
1168 doi.org/10.1007/s10661-013-3143-1.
1169 Thomas, K. E., R. I. Hall, and G. J. Scrimgeour. 2015. Relations between water physico-
1170 chemistry and benthic algal communities in a northern Canadian watershed: defining
1171 reference conditions using multiple descriptors of community structure. Environ. Monit.
1172 Assess. **187**: 564. doi:10.1007/s10661-015-4778-x
1173 Van Nieuwenhuyse, E. E., and J. R. Jones. 1996. Phosphorus–chlorophyll relationship in
1174 temperate streams and its variation with stream catchment area. Can. J. Fish. Aquat. Sci.
1175 **53**: 99–105.
1176 Vannote, R. L., W. G. Minshall, K. W. Cummins, J. R. Sedell, and C. E. Cushing. 1980. The
1177 River Continuum Concept. Can. J. Fish. Aquat. Sci. **37**: 130–137. doi:10.1139/f80-017

Varol, M., and B. Şen. 2018. Abiotic factors controlling the seasonal and spatial patterns of phytoplankton community in the Tigris River, Turkey. River Res. Appl. **34**: 13–23. doi:10.1002/rra.3223

Visser, P. M., J. M. Verspagen, G. Sandrini, L. J. Stal, H. C. Matthijs, T. W. Davis, H. W. Paerl, and J. Huisman. 2016. How rising CO_2 and global warming may stimulate harmful cyanobacterial blooms. Harmful Algae **54**: 145–159. doi:10.1016/j.hal.2015.12.006

Vinebrooke, R .D., and P. R. Leavitt. 1999. Phytobenthos and phytoplankton as potential indicators of climate change in mountain lakes and ponds: a HPLC-based pigment approach. J. N. Am. Benthol. Soc. **18**: 14-32. doi.org/10.2307/1468006

Vogt, R. J., J. A. Rusak, A. Patoine, and P. R. Leavitt. 2011. Differential effects of energy and mass influx on the landscape synchrony of lake ecosystems. Ecology **92**: 1104-1114. doi.org/10.1890/10-1846.1

Vogt, R. J., S. Sharma, and P. R. Leavitt. 2018. Direct and interactive effects of climate, meteorology, river hydrology, and lake characteristics on water quality in productive lakes of the Canadian Prairies. Can. J. Fish. Aquat. Sci. **75**: 47-59. doi:10.1139/cjfas-2016-0520

Waiser, M. J., V. Tumber, and J. Holm. 2011. Effluent-dominated streams. Part 1: Presence and effects of excess nitrogen and phosphorus in Wascana Creek, Saskatchewan, Canada. Environ. Toxicol. Chem. **30**: 496–507. doi:10.1002/etc.399

Walsh, C. J. 2000. Urban impacts on the ecology of receiving waters: A framework for assessment, conservation and restoration. Hydrobiologia **431**: 107–114. doi:10.1023/a:1004029715627

Walsh, C. J., A. H. Roy, J. W. Feminella, P. D. Cottingham, P. M. Groffman, and R. P. Morgan. 2005. The urban stream syndrome: current knowledge and the search for a cure. J. N. Am. Benthol. Soc. **24**: 706–723. doi:10.1899/04-028.1

Walsh, W. G., and V. Wepener. 2009. The influence of land use on water quality and diatom community structures in urban and agriculturally-stressed rivers. Water S. A. **35**: 579-594. doi:10.4314/wsa.v35i5.49184

Wehr, J. D., and J. P. Descy, J. P. 1998. Use of phytoplankton in large river management. J. Phycol., **34**: 741–749.

Weigelhofer, G., N. Welti, and T. Hein. 2013. Limitations of stream restoration for nitrogen retention in agricultural headwater streams. Ecol. Eng. **60**: 224–234.

Welch, E. B., J. M. Jacoby, R. R. Horner, and M. R. Seeley. 1988. Nuisance biomass levels of periphytic algae in streams. Hydrobiologia **157**: 161–168. doi:10.1007/bf00006968

Wickham H. 2016. *ggplot2: Elegant Graphics for Data Analysis*. Springer-Verlag New York. ISBN 978-3-319-24277-4, https://ggplot2.tidyverse.org.

Wood, S. N. 2011. Fast stable restricted maximum likelihood and marginal likelihood estimation of semiparametric generalized linear models. J. Roy. Stat. Soc. B Stat. Methodol. **73**: 3–36. doi:10.1111/j.1467-9868.2010.00749.x

Wood, S. N. 2017. Generalized Additive Models: An Introduction with R, 2 edition, Chapman and Hall/CRC.

Wood, S. N., N. Pya, and B. Säfken. 2015. Smoothing parameter and model selection for general smooth models. J. Am. Stat. Assoc. **111**: 1548–1563. doi:10.1080/01621459.2016.1180986

Wu, N., B. Schmalz, and N. Fohrer. 2011. Distribution of phytoplankton in a German lowland river in relation to environmental factors. J. Plankton Res. **33**: 807–820. doi:10.1093/plankt/fbq139

Wurtsbaugh, W. A., H. W. Paerl, and W. K. Dodds. 2019. Nutrients, eutrophication and harmful algal blooms along the freshwater to marine continuum. WIRE Wat. **6**: e1373. doi:10.1002/wat2.1373

Yu, Q., Y. Chen, Z. Liu, N. de Giesen, and D. Zhu. 2015. The influence of a eutrophic lake to the river downstream: Spatiotemporal algal composition changes and the driving factors. Water **7**: 2184–2201. doi:10.3390/w7052184

Table 1. The spatial physico-chemical values (mean ± standard error) at each stream location and the wastewater treatment plant (WWTP) from May to September in 2018 and 2019. Note that WWTP turbidity is the mean and standard error in 2017 because turbidity was not taken in 2018 and 2019, but values are expected to be similar to 2017. Salinity in g total dissolved solids L^{-1}. Nutrients include total dissolved nitrogen (TDN), nitrate (NO_3^-), ammonium (NH_4^+), total dissolved phosphorus (TDP), soluble reactive phosphorus (SRP), and stable nitrogen isotope ratio ($\delta^{15}N$).

Site	1	2	3	4	5	6	7	8	9	WWTP
Distance to WWTP (km)	-43	-7	4	36	60	-	69	104	137	0
Discharge (m^3 s^{-1})	0.06 ± 0.03	0.58 ± 0.24	1.18 ± 0.21	1.34 ± 0.32	1.42 ± 0.52	3.08 ± 0.81	4.29 ± 0.88	2.90 ± 0.17	3.68 ± 0.17	0.81 ± 0.01
Turbidity (NTU)	4.97 ± 0.54	24.33 ± 2.32	7.39 ±1.08	12.52 ± 2.53	18.51 ± 4.39	38.30 ± 3.99	32.98 ± 4.55	30.99 ± 3.83	40.03 ± 4.60	4.45 ± 0.27
Secchi (cm)	63.35 ± 7.59	20.04 ± 1.31	53.46 ± 2.99	50.68 ± 5.27	37.66 ± 4.13	16.94 ± 1.08	21.69 ± 1.60	19.86 ± 2.11	17.83 ± 3.04	-
pH	8.60 ± 0.13	8.42 ± 0.08	7.77 ± 0.06	8.84 ± 0.10	8.66 ±0.09	8.49 ± 0.06	8.52 ± 0.05	8.61 ±0.09	8.77 ±0.07	7.42 ± 0.01
Salinity (g L^{-1})	1.03 ± 0.05	0.45 ±0.02	0.72 ± 0.04	0.71 ± 0.04	0.75 ± 0.03	0.38 ± 0.02	0.51 ± 0.04	0.60 ± 0.05	0.58 ± 0.05	-
Specific conductance (µS cm^{-1})	1999.55 ± 82.07	910.49 ± 48.54	1436.00 ± 62.43	1412.29 ± 80.95	1468.30 ± 65.59	757.34 ± 40.45	1055.35 ± 78.43	1203.30 ± 100.34	1182.80 ± 90.24	-
Temperature (°C)	16.88 ± 0.82	17.49 ± 0.84	17.95 ± 0.70	18.75 ± 0.80	18.16 ± 0.85	18.06 ± 0.81	18.28 ± 0.83	17.83 ± 0.78	17.56 ±0.78	20.07 ± 0.14
TDN (mg N L^{-1})	1.75 ± 0.14	0.99 ± 0.06	5.53 ± 0.52	3.19 ± 0.42	2.83 ± 0.40	0.62 ± 0.04	1.52 ± 0.30	1.00 ± 0.11	0.93 ± 0.09	10.62 ± 0.12
NO_3^- (mg N L^{-1})	0.02 ± 0.01	0.05 ± 0.01	1.88 ± 0.24	1.21 ± 0.25	1.02 ± 0.24	0.02 ± 0.01	0.38 ± 0.10	0.12 ± 0.04	0.04 ± 0.01	5.80 ± 0.07
NH_4^+ (mg N L^{-1})	0.03 ± 0.01	0.11 ± 0.03	0.89 ± 0.21	0.11 ± 0.03	0.14 ± 0.09	0.05 ± 0.03	0.04 ± 0.01	0.06 ± 0.03	0.06 ± 0.03	1.82 ± 0.07
$\delta^{15}N$ (‰)	4.93 ± 0.28	5.73 ± 0.66	15.22 ± 0.73	13.63 ± 0.78	13.97 ± 1.04	5.26 ± 0.84	11.00 ± 1.02	7.61 ± 0.50	6.27 ± 0.41	16.82 ± 0.28
TDP (mg P L^{-1})	0.38 ± 0.07	0.09 ± 0.01	0.21 ± 0.04	0.12 ± 0.01	0.13 ± 0.01	0.04 ± 0.01	0.08 ± 0.01	0.05 ± 0.01	0.04 ± 0.01	0.58 ± 0.02
SRP (mg P L^{-1})	0.25 ± 0.05	0.05 ± 0.01	0.08 ± 0.01	0.065 ± 0.01	0.07 ± 0.01	0.03 ± 0.01	0.05 ± 0.01	0.03 ± 0.01	0.02 ± 0.01	-
TDN:SRP	13.78 ± 2.68	37.83 ± 8.29	79.85 ± 11.22	86.85 ± 26.67	74.10 ± 16.46	45.31 ± 5.72	55.95 ± 10.99	59.70 ± 8.52	65.94 ± 12.15	-

1239 **Figure legends**

1240 **Fig. 1.** Map of sampling sites within Wascana Creek (WC, main panel), the Qu'Appelle River
1241 (QR, lower right) and Saskatchewan, Canada (SK, upper right). Sampling location in white
1242 circles, hydrometric stations in red triangles, and City of Regina (yellow outline) wastewater
1243 treatment plant as yellow diamond.

1244 **Fig. 2.** The modelled spatial and temporal distribution of physico-chemical covariates in 2018
1245 and 2019 in Wascana Creek and Qu'Appelle River along a continuum in reference to Regina's
1246 wastewater treatment plant (WWTP). Modelled physical-chemical variables and their explained
1247 deviance included: discharge (67.6%), turbidity (82.2% for 2018, 80.0% for 2019), Secchi depth
1248 (75.5%), pH (78.4%), salinity (80.1%), specific conductance (77.6%), temperature (87.7%),
1249 TDN (87.4%), NO_3^- (79.3%), NH_4^+ (64.6%), $\delta^{15}N$ (83.0%), TDP (70.3%), SRP (78.0%), and
1250 TDN:SRP (85.6%). Note that turbidity was modelled separately each year because adding 2019
1251 obscured the 2018 spatiotemporal distribution. Coloured lines are predicted means at four days
1252 of year (DOY 136, 170, 200, 236) that correspond to summer months in the growing season.
1253 Shaded areas are 95% confidence intervals. Square boxes and error bars are the monthly mean
1254 and confidence intervals, respectively, of a control site in QR ~5 km upstream of the WC-QR
1255 continuum that was not modelled. Red and black dotted lines represent the inflow of WWTP
1256 effluent into WC and the confluence of WC with QR, respectively. The red horizontal line in the
1257 TDN:SRP panel is at 23 above which P-limitation occurs.

1258 **Fig. 3.** The modelled spatial and temporal distribution of total suspended (phytoplankton, a) and
1259 benthic (epilithon, b) algae and cyanobacteria and their ratio (c), using trichromatic chlorophyll a
1260 as a proxy, in 2018 (top) and 2019 (bottom) in Wascana Creek (WC) and Qu'Appelle River
1261 (QR) along a continuum in reference to Regina's wastewater treatment plant (WWTP). The

phytoplankton model explained 62.6%, the epilithon model explained 45.5% deviance, and the ratio model explained 53.9% of deviance. Coloured lines are predicted means at four days of year, 136, 170, 200, 236, which correspond to months in the growing season. Shaded areas are 95% confidence intervals. Square boxes and error bars are the monthly mean and confidence intervals, respectively, of a control site in QR ~5 km upstream of the WC-QR continuum that was not modelled. Red and black dotted lines represent the inflow of WWTP effluent into WC and the confluence of WC with QR, respectively.

Fig. 4. The modelled spatial and temporal distribution of suspended (phytoplankton, a) and benthic (periphyton, b) algae and cyanobacteria pigments and their ratio (c), using carotenoid HPLC, in 2018 and 2019 in Wascana Creek (WC) and Qu'Appelle River (QR) along a continuum in reference to Regina's wastewater treatment plant. Modelled taxa by pigment include siliceous algae (fucoxanthin), cryptophytes (alloxanthin), chlorophytes (chlorophyll b), and total cyanobacteria (echinenone). Deviance explained was 87% for phytoplankton, 81% for periphyton pigments, and 77.5% for their ratio. Coloured lines are predicted means at four days of year, 136, 170, 200, 236, in 2018 and 2019 that correspond to summer months in the growing season. Shaded areas are 95% confidence intervals. Red and black dotted lines represent the inflow of WWTP effluent into WC and the confluence of WC with QR, respectively.

Fig. 5. The modelled marginal smooth effects of physico-chemical variables on total phytoplankton (a) and periphyton (b) biomass (trichromatic Chl a) in Wascana Creek (WC) and the Qu'Appelle River (QR) in 2018 and 2019. Red lines represent the mean effect. Blue shaded areas are 95% credible intervals. Deviance explained for the phytoplankton and epilithon models was 66.3% and 53.9%, respectively. P-values are located at the top of each plot. Temperature

and TDN:SRP were non-significant (not presented). Turbidity was removed due to covariation with Secchi depth.

Fig. 6. The modelled marginal smooth effects of physico-chemical variables on phytoplankton (a) and epilithon (b) pigments in Wascana Creek (WC) and the Qu'Appelle River (QR) in 2018 and 2019. Deviance explained for the phytoplankton and epilithon models was 84.0% and 72.6%, respectively. For the global pigment smooths (all pigments included) red lines represent the mean effect and blue shaded areas are 95% credible intervals. The taxa-specific effects (how the specific pigments vary over the global effect) are to the right of the global effect panels and shaded areas are 95% credible intervals. Siliceous algae (fucoxanthin) are in orange, cryptophytes (alloxanthin) are in yellow, chlorophytes (chl b) are in green, and cyanobacteria (echinenone) are in blue. P-values are located at the top of each plot. Turbidity was removed due to covariation with Secchi depth.

1296

1297

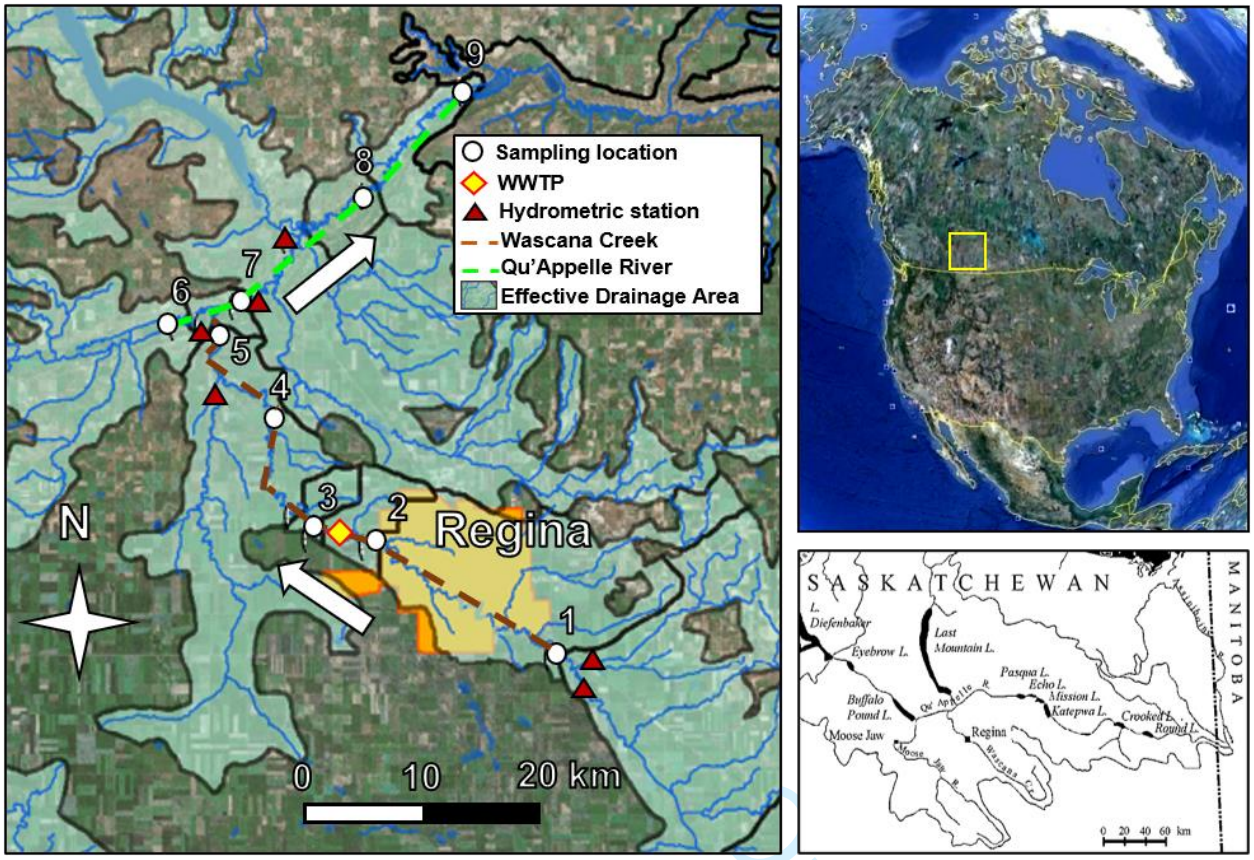

1298

1299 **Fig. 1.** Map of sampling sites within Wascana Creek (WC, main panel), the Qu'Appelle River

1300 (QR, lower right) and Saskatchewan, Canada (SK, upper right). Sampling location in white

1301 circles, hydrometric stations in red triangles, and City of Regina (yellow outline) wastewater

1302 treatment plant as yellow diamond.

1303

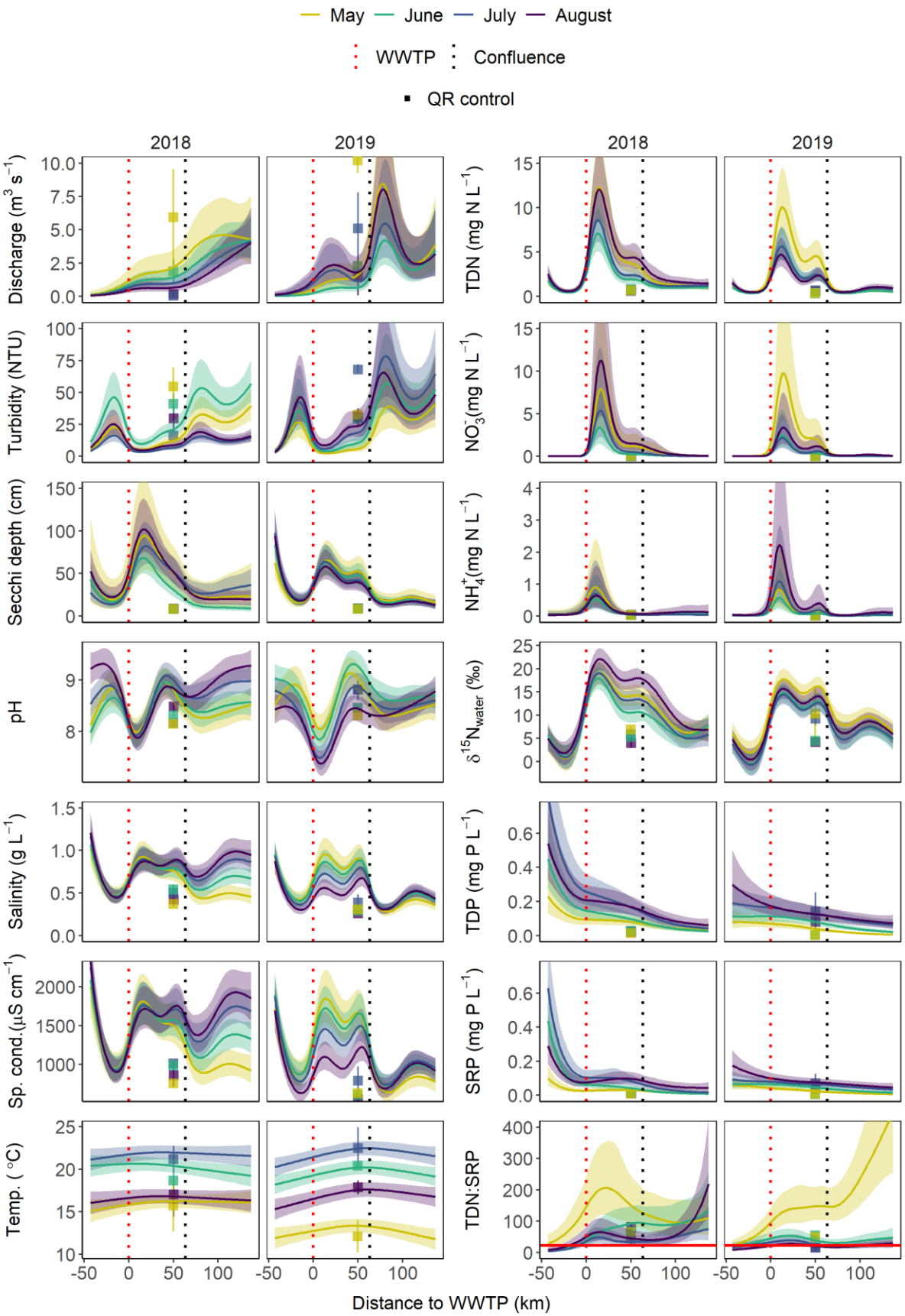
May
June
July
August
WWTP
Confluence
QR control
2018
2019
Discharge (m^3 s^{-1})
Turbidity (NTU)
Secchi depth (cm)
pH
Salinity (g L^{-1})
Sp. cond.(µS cm^{-1})
Temp. (°C)
TDN (mg N L^{-1})
NO_3^-(mg N L^{-1})
NH_4^+(mg N L^{-1})
$\delta^{15}N_{water}$ (‰)
TDP (mg P L^{-1})
SRP (mg P L^{-1})
TDN:SRP
Distance to WWTP (km)

1304 **Fig. 2**

Fig. 2. The modelled spatial and temporal distribution of physico-chemical covariates in 2018 and 2019 in Wascana Creek and Qu'Appelle River along a continuum in reference to Regina's wastewater treatment plant (WWTP). Modelled physical-chemical variables and their explained deviance included: discharge (67.6%), turbidity (82.2% for 2018, 80.0% for 2019), Secchi depth (75.5%), pH (78.4%), salinity (80.1%), specific conductance (77.6%), temperature (87.7%), TDN (87.4%), NO_3^- (79.3%), NH_4^+ (64.6%), $\delta^{15}N$ (83.0%), TDP (70.3%), SRP (78.0%), and TDN:SRP (85.6%). Note that turbidity was modelled separately each year because adding 2019 obscured the 2018 spatiotemporal distribution. Coloured lines are predicted means at four days of year (DOY 136, 170, 200, 236) that correspond to summer months in the growing season. Shaded areas are 95% confidence intervals. Square boxes and error bars are the monthly mean and confidence intervals, respectively, of a control site in QR ~5 km upstream of the WC-QR continuum that was not modelled. Red and black dotted lines represent the inflow of WWTP effluent into WC and the confluence of WC with QR, respectively. The red horizontal line in the TDN:SRP panel is at 23 above which P-limitation occurs.

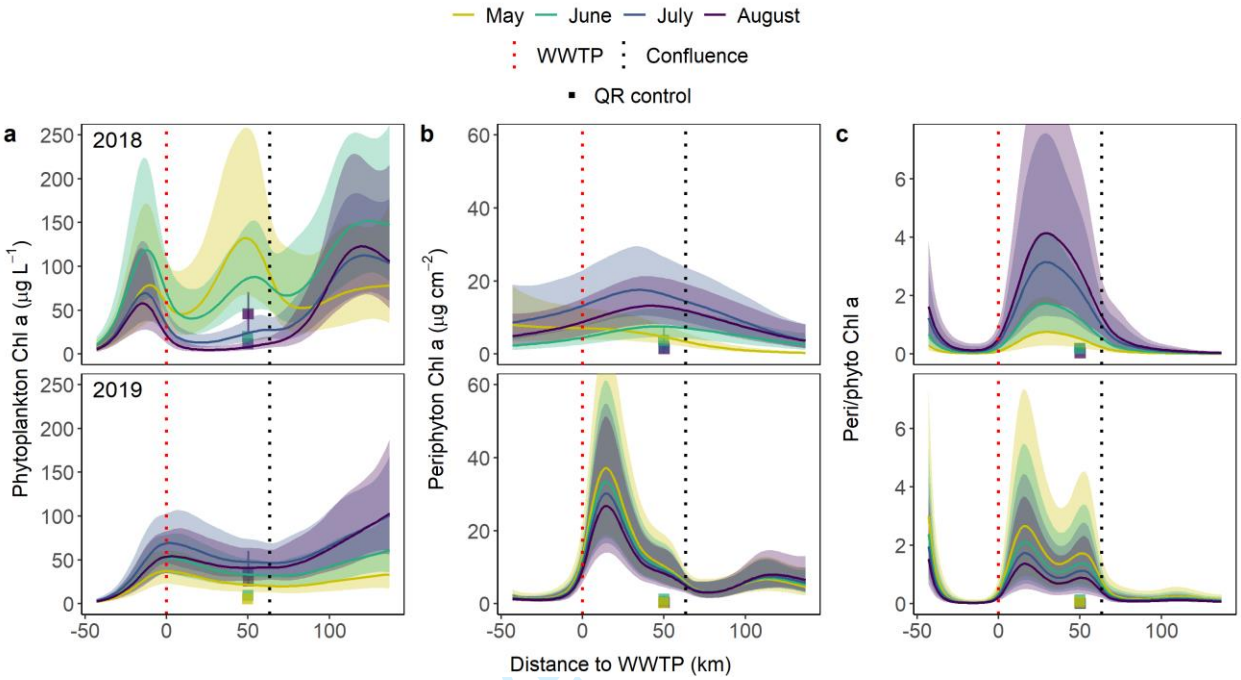

Fig. 3. The modelled spatial and temporal distribution of total suspended (phytoplankton, a) and benthic (epilithon, b) algae and cyanobacteria and their ratio (c), using trichromatic chlorophyll a as a proxy, in 2018 (top) and 2019 (bottom) in Wascana Creek (WC) and Qu'Appelle River (QR) along a continuum in reference to Regina's wastewater treatment plant (WWTP). The phytoplankton model explained 62.6%, the epilithon model explained 45.5% deviance, and the ratio model explained 53.9% of deviance. Coloured lines are predicted means at four days of year, 136, 170, 200, 236, which correspond to months in the growing season. Shaded areas are 95% confidence intervals. Square boxes and error bars are the monthly mean and confidence intervals, respectively, of a control site in QR ~5 km upstream of the WC-QR continuum that was not modelled. Red and black dotted lines represent the inflow of WWTP effluent into WC and the confluence of WC with QR, respectively.

1334

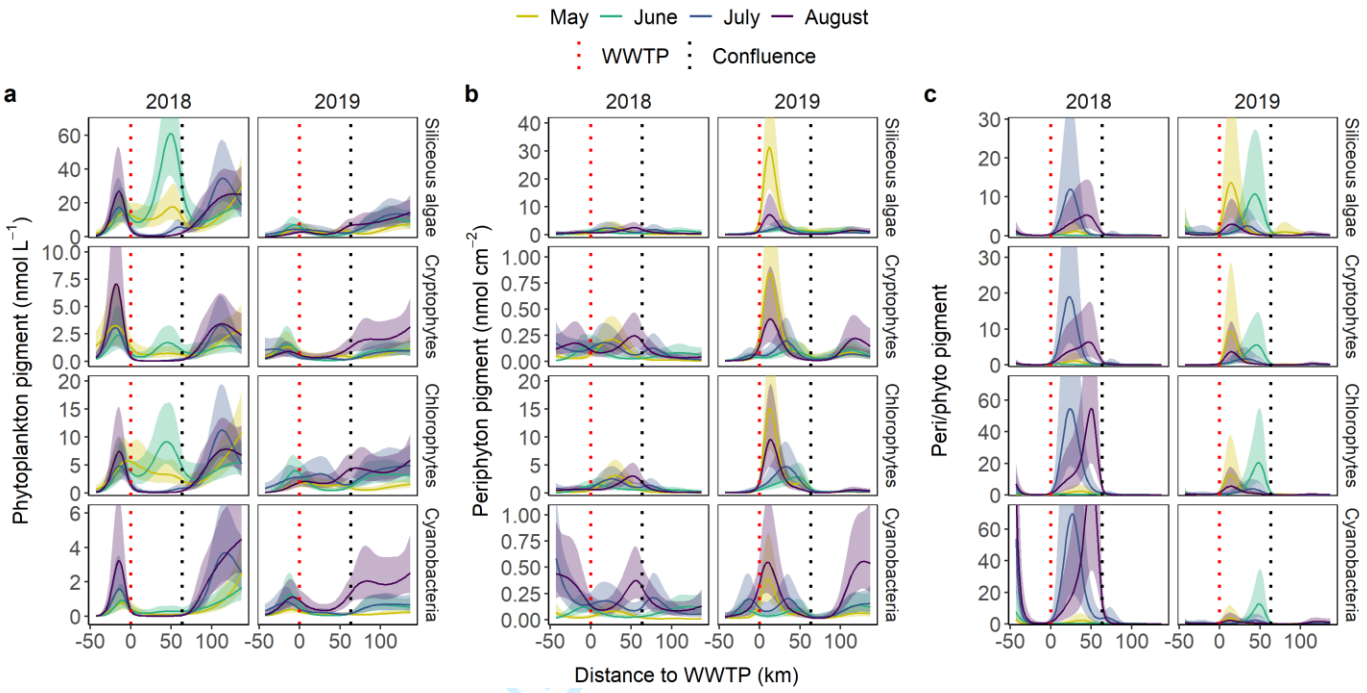

1335

1336 **Fig. 4.** The modelled spatial and temporal distribution of suspended (phytoplankton, a) and

1337 benthic (periphyton, b) algae and cyanobacteria pigments and their ratio (c), using carotenoid

1338 HPLC, in 2018 and 2019 in Wascana Creek (WC) and Qu'Appelle River (QR) along a

1339 continuum in reference to Regina's wastewater treatment plant. Modelled taxa by pigment

1340 include siliceous algae (fucoxanthin), cryptophytes (alloxanthin), chlorophytes (chlorophyll b),

1341 and total cyanobacteria (echinenone). Deviance explained was 87% for phytoplankton, 81% for

1342 periphyton pigments, and 77.5% for their ratio. Coloured lines are predicted means at four days

1343 of year, 136, 170, 200, 236, in 2018 and 2019 that correspond to summer months in the growing

1344 season. Shaded areas are 95% confidence intervals. Red and black dotted lines represent the

1345 inflow of WWTP effluent into WC and the confluence of WC with QR, respectively.

1346

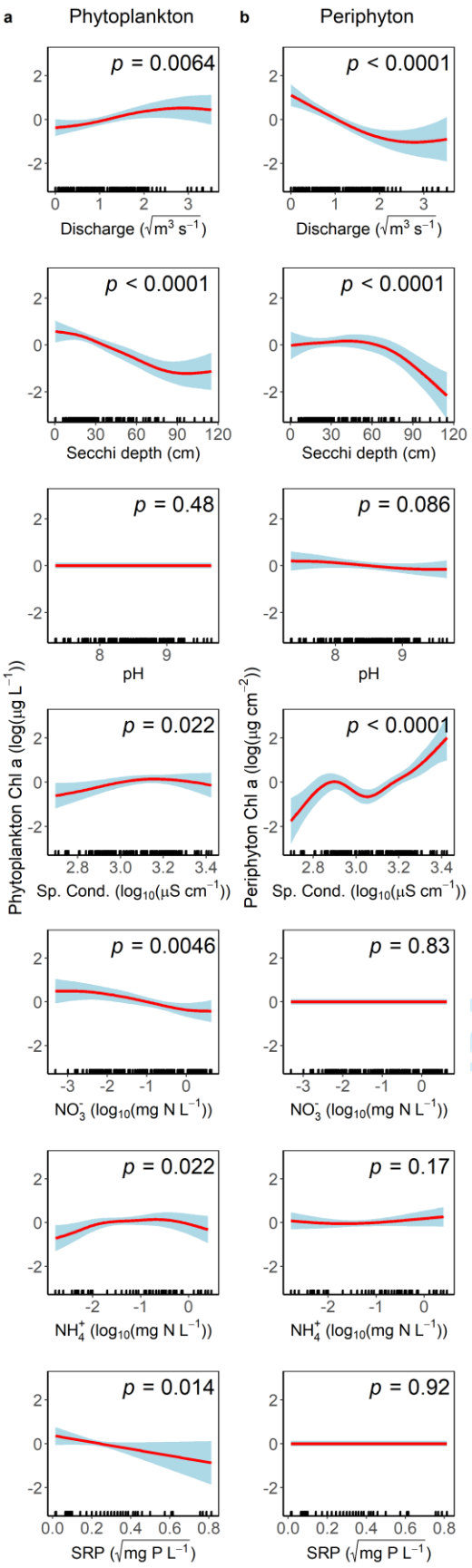
a
Phytoplankton
b
Periphyton
p = 0.0064
p < 0.0001
Discharge (√m³ s⁻¹)
p < 0.0001
p < 0.0001
Secchi depth (cm)
p = 0.48
p = 0.086
pH
Phytoplankton Chl a (log(µg L⁻¹))
Periphyton Chl a (log(µg cm⁻²))
p = 0.022
p < 0.0001
Sp. Cond. (log10(µS cm⁻¹))
p = 0.0046
p = 0.83
NO3- (log10(mg N L⁻¹))
p = 0.022
p = 0.17
NH4+ (log10(mg N L⁻¹))
p = 0.014
p = 0.92
SRP (√mg P L⁻¹)

1347 **Fig. 5**

Fig. 5. The modelled marginal smooth effects of physico-chemical variables on total phytoplankton (a) and periphyton (b) biomass (trichromatic Chl a) in Wascana Creek (WC) and the Qu'Appelle River (QR) in 2018 and 2019. Red lines represent the mean effect. Blue shaded areas are 95% credible intervals. Deviance explained for the phytoplankton and epilithon models was 66.3% and 53.9%, respectively. P-values are located at the top of each plot. Temperature and TDN:SRP were non-significant (not presented). Turbidity was removed due to covariation with Secchi depth.

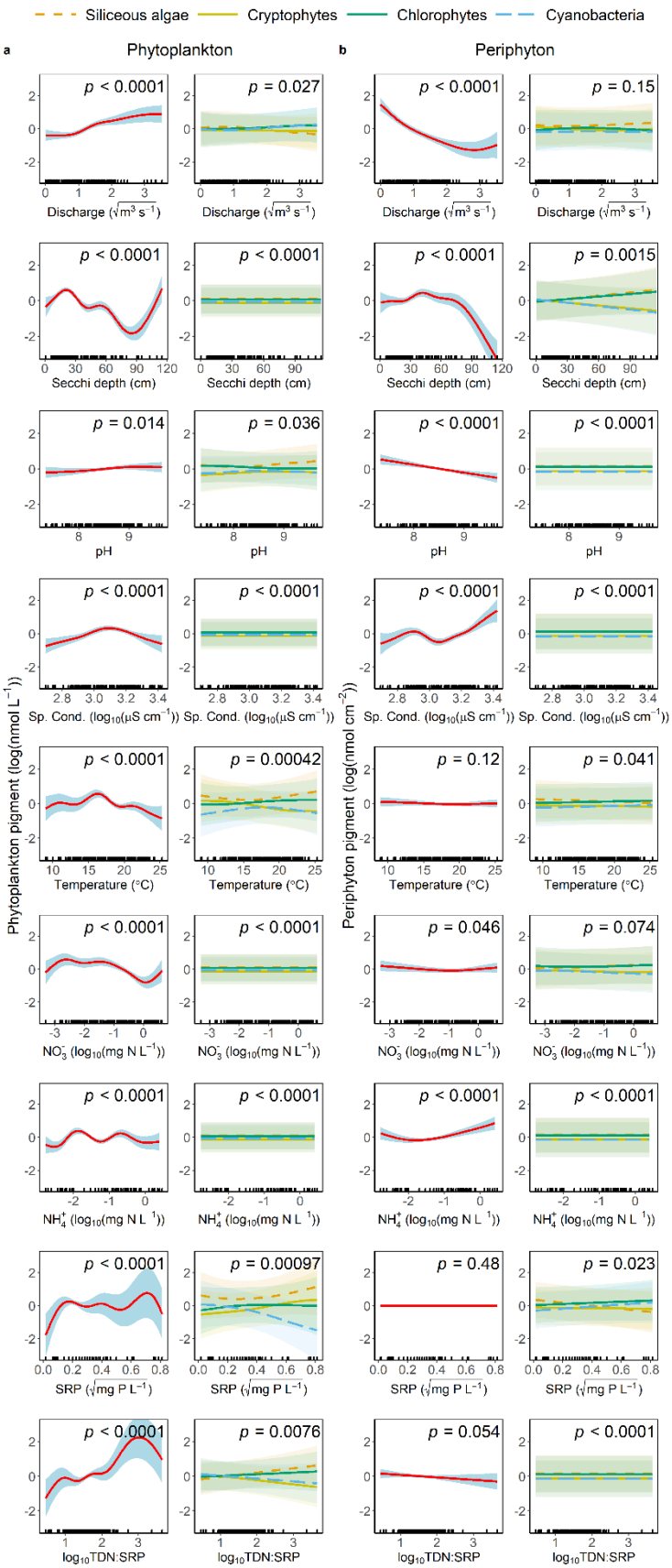
Siliceous algae
Cryptophytes
Chlorophytes
Cyanobacteria
a
Phytoplankton
b
Periphyton
Phytoplankton pigment (log(nmol L⁻¹))
Periphyton pigment (log(nmol cm⁻²))
p < 0.0001
p = 0.027
p < 0.0001
p = 0.15
Discharge (√m³ s⁻¹)
p < 0.0001
p < 0.0001
p < 0.0001
p = 0.0015
Secchi depth (cm)
p = 0.014
p = 0.036
p < 0.0001
p < 0.0001
pH
p < 0.0001
p < 0.0001
p < 0.0001
p < 0.0001
Sp. Cond. (log10(µS cm⁻¹))
p < 0.0001
p = 0.00042
p = 0.12
p = 0.041
Temperature (°C)
p < 0.0001
p < 0.0001
p = 0.046
p = 0.074
NO3⁻ (log10(mg N L⁻¹))
p < 0.0001
p < 0.0001
p < 0.0001
p < 0.0001
NH4⁺ (log10(mg N L⁻¹))
p < 0.0001
p = 0.00097
p = 0.48
p = 0.023
SRP (√mg P L⁻¹)
p < 0.0001
p = 0.0076
p = 0.054
p < 0.0001
log10TDN:SRP

1355 **Fig. 6.**

Fig. 6. The modelled marginal smooth effects of physico-chemical variables on phytoplankton (a) and epilithon (b) pigments in Wascana Creek (WC) and the Qu'Appelle River (QR) in 2018 and 2019. Deviance explained for the phytoplankton and epilithon models was 84.0% and 72.6%, respectively. For the global pigment smooths (all pigments included) red lines represent the mean effect and blue shaded areas are 95% credible intervals. The taxa-specific effects (how the specific pigments vary over the global effect) are to the right of the global effect panels and shaded areas are 95% credible intervals. Siliceous algae (fucoxanthin) are in orange, cryptophytes (alloxanthin) are in yellow, chlorophytes (chl b) are in green, and cyanobacteria (echinenone) are in blue. P-values are located at the top of each plot. Turbidity was removed due to covariation with Secchi depth.

1367 **Supporting Information**

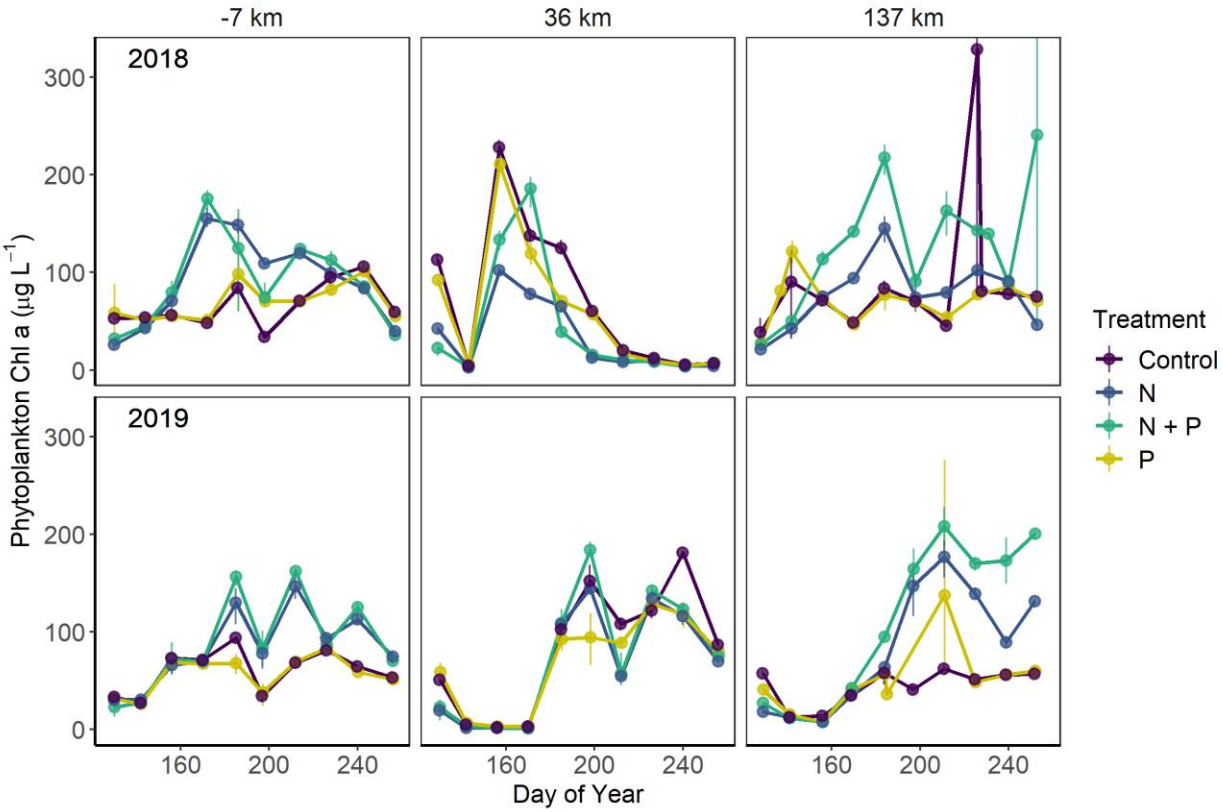

1368

1369 **Fig. S1.** Phytoplankton nutrient experiments for 2018 and 2019 done across the sampling season

1370 (May to September) for three sites: 7 km upstream of the wastewater treatment plant (WWTP),

1371 36 km (in Wascana Creek) and 137 km (in Qu'Appelle River) downstream of the WWTP. Each

1372 point is the mean of three replicates and error bars are 95% confidence intervals.

1373

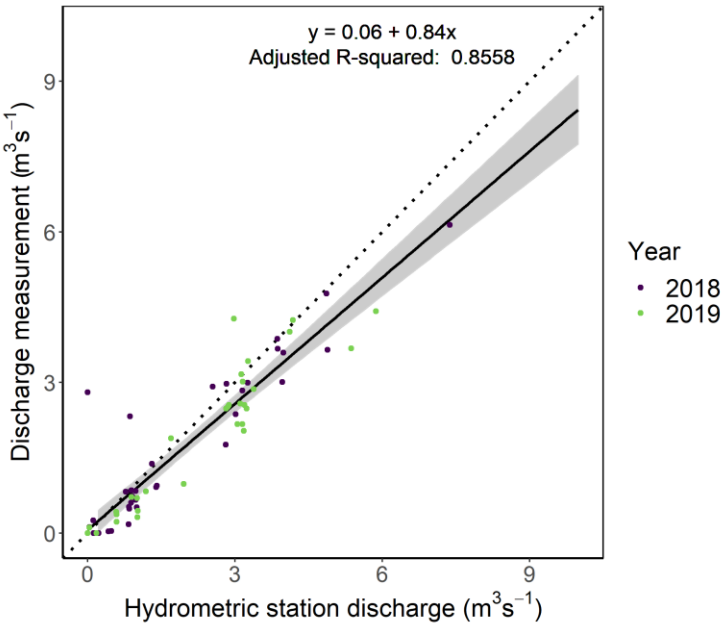

1374

1375 **Fig. S2**. A comparison of discharge (m^3 s^{-1}) measured in the field and discharge estimated from

1376 hydrometric stations in 2018 and 2019.

1377

1378

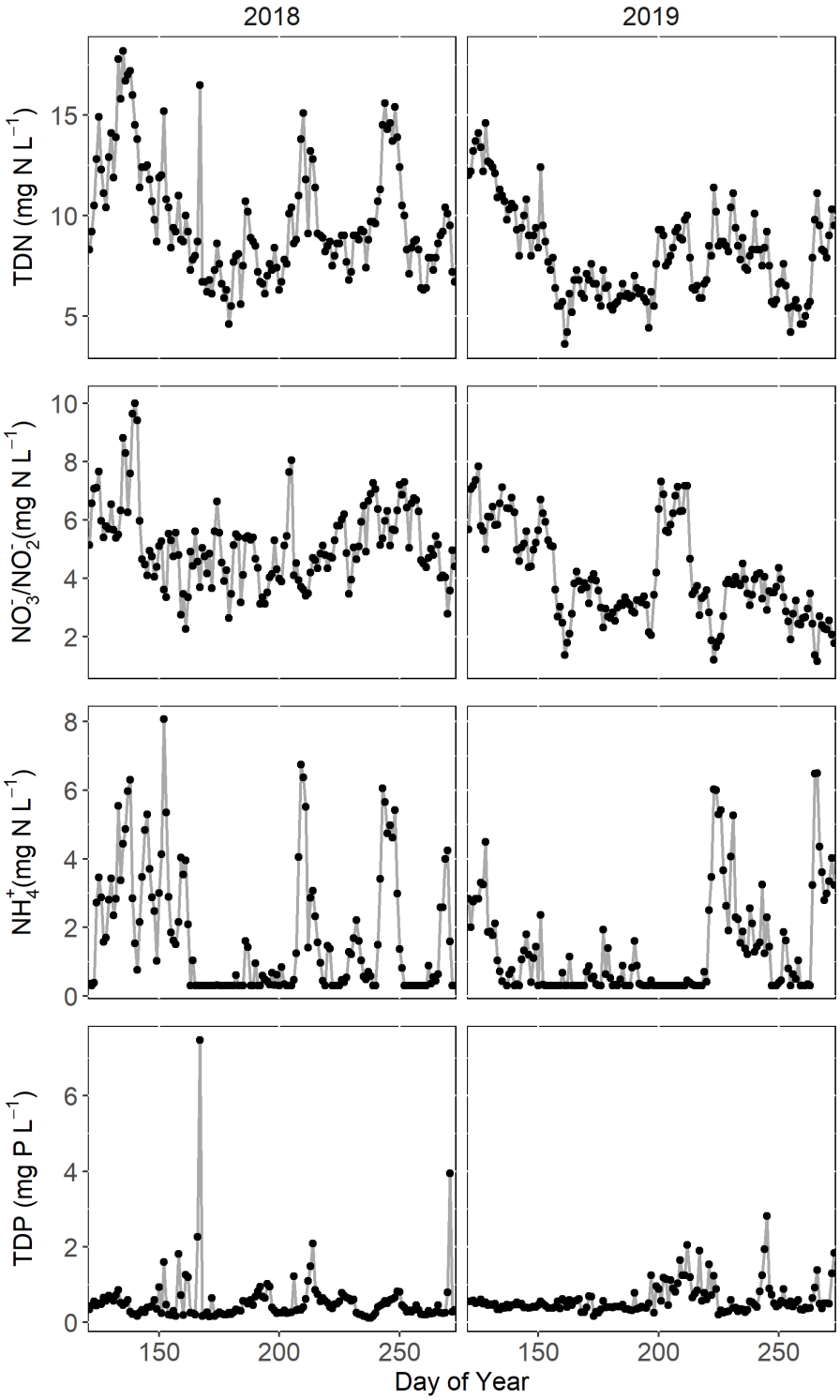

Fig. S3. Final treated effluent nutrient concentrations in the growing season (May to September) in 2018 and 2019.

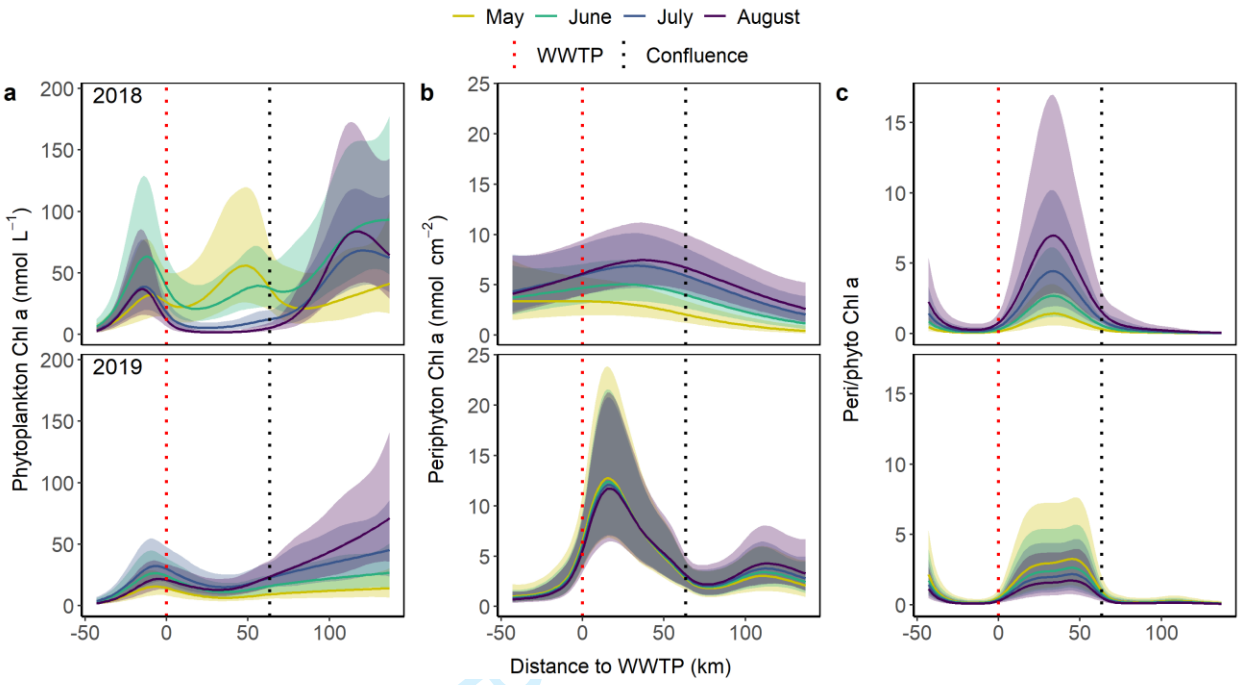

1381

1382

1383 **Fig. S4.** The modelled spatial and temporal distribution of total suspended (phytoplankton, a)
1384 and benthic (epilithon, b) algae and cyanobacteria and their ratio (c), using HPLC chlorophyll a
1385 as a proxy, in 2018 (top) and 2019 (bottom) in Wascana Creek and Qu'Appelle River along a
1386 continuum in reference to Regina's wastewater treatment plant. The phytoplankton model
1387 explained 60.9%, the epilithon model explained 34.0% deviance, and the ratio model explained
1388 51.9% of deviance. Coloured lines are predicted means at four days of year (DOY 136, 170,
1389 200, 236) that correspond to summer months in the growing season. Shaded areas are 95%
1390 confidence intervals. Red and black dotted lines represent the inflow of effluent into WC and the
1391 confluence of WC with QR, respectively.

1392

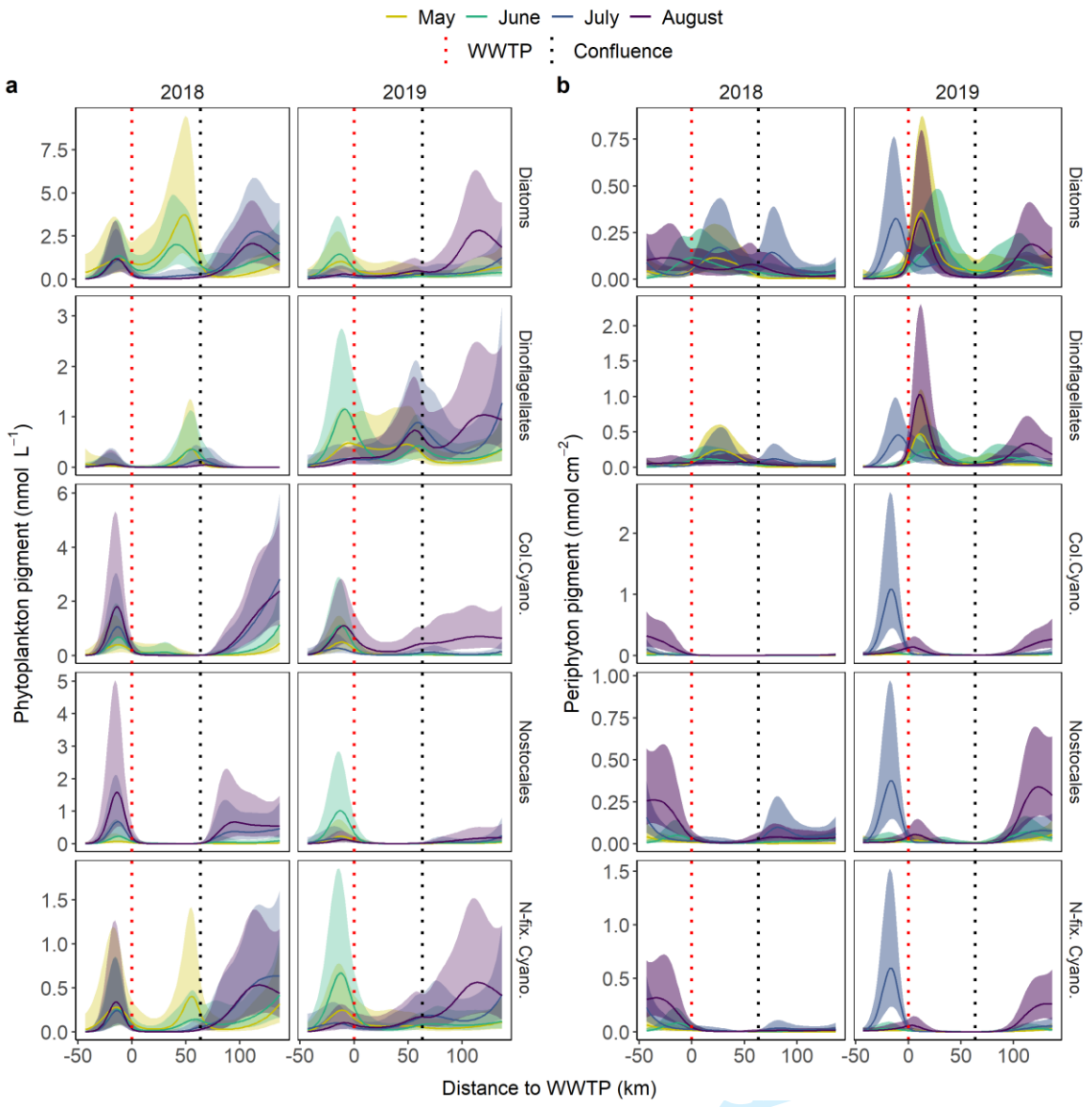

Fig. S5. The spatiotemporal distribution of other HPLC pigments: diatoxanthin (diatoms), diadinoxanthin (dinoflagellates), myxoxanthophyll (colonial cyanobacteria), canthaxanthin (Nostocales), and aphanizophyll (N-fixing cyanobacteria). The phytoplankton model explained 61.6% and the epilithon model explained 63.0% deviance. Coloured lines are predicted means at four days of year (DOY 136, 170, 200, 236) that correspond to summer months in the growing season. Shaded areas are 95% confidence intervals. Red and black dotted lines represent the inflow of effluent into WC and the confluence of WC with QR, respectively.

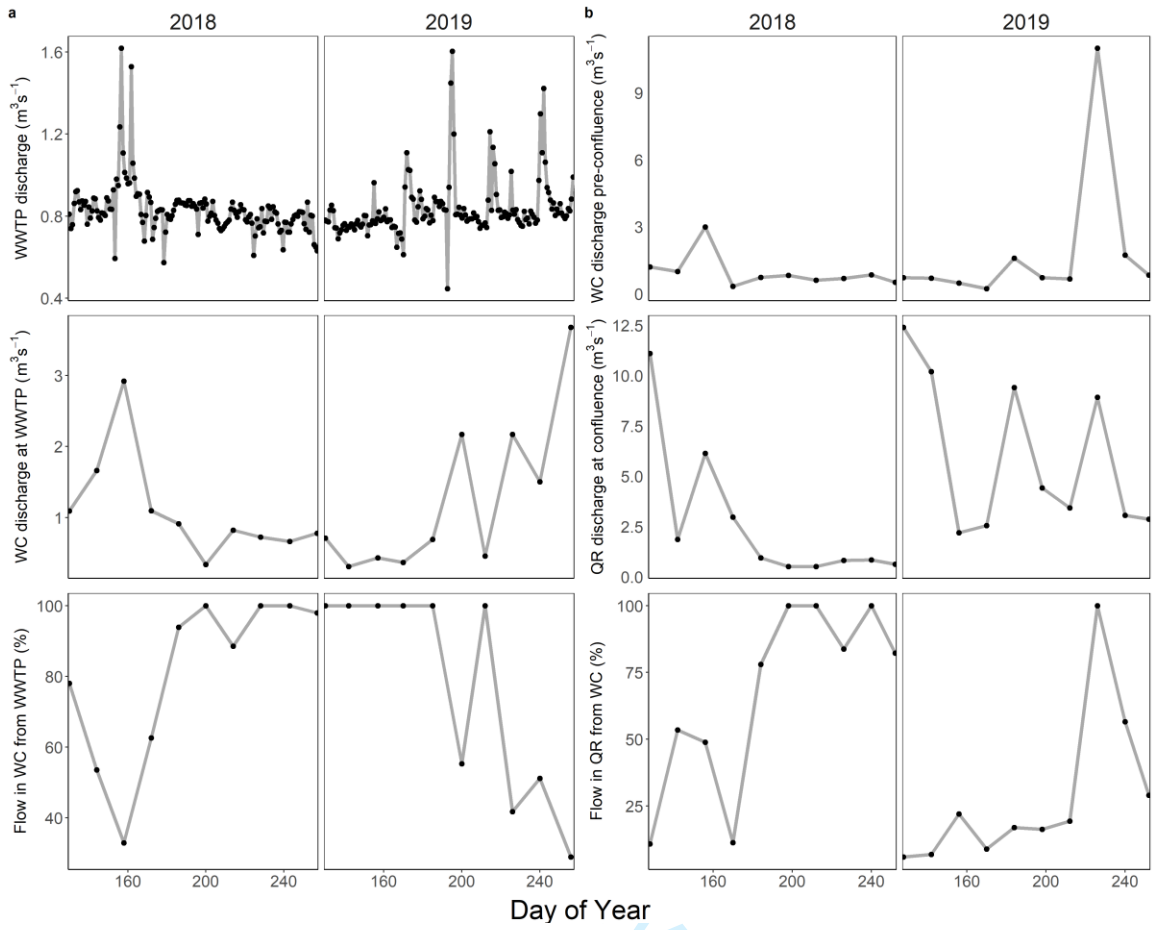

1401

1402 **Fig. S6.** Flow in Wascana Creek, Saskatchewan, attributable to the Regina wastewater treatment

1403 plant (WWTP) (a) and flow in QR attributable to WC (b) across the growing season (May to

1404 September) in 2018 and 2019.

1405

1406

1407 **Fig. S7.** Photographs of study streams in (a) headwater, (b) effluent-impacted, and (c) post-

1408 confluence reaches. Insets illustrate epilithic periphyton development.

1409

a.

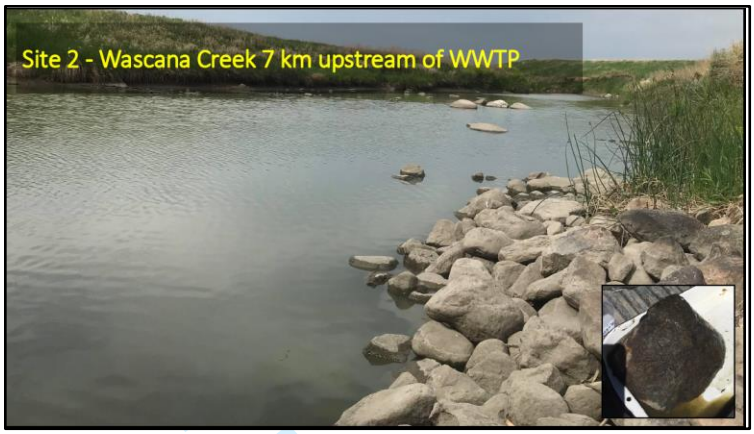

b.

c.

1410

1411

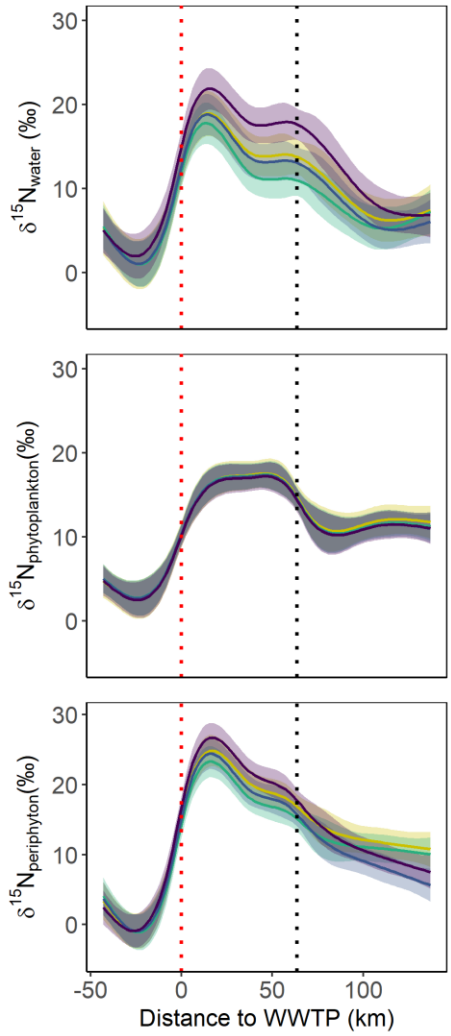

1412

1413 **Fig. S8.** The modelled spatial and temporal distribution of water, phytoplankton, and periphyton
1414 nitrogen isotopes in Wascana Creek and Qu'Appelle River along a continuum in reference to
1415 Regina's wastewater treatment plant. The water, phytoplankton, and periphyton N isotope
1416 models explained 82.4%, 77.5%, and 92.0% of deviance. Coloured lines are predicted means at
1417 four days of year (DOY 136, 170, 200, 236) that correspond to summer months in the growing
1418 season. Shaded areas are 95% confidence intervals. Red and black dotted lines represent the
1419 inflow of effluent into WC and the confluence of WC with QR, respectively.